creative commons
COMMONS DEED

저작자표시-비영리-변경금지 2.0 대한민국

이용자는 아래의 조건을 따르는 경우에 한하여 자유롭게

- 이 저작물을 복제, 배포, 전송, 전시, 공연 및 방송할 수 있습니다.

다음과 같은 조건을 따라야 합니다:



저작자표시. 귀하는 원저작자를 표시하여야 합니다.



비영리. 귀하는 이 저작물을 영리 목적으로 이용할 수 없습니다.



변경금지. 귀하는 이 저작물을 개작, 변형 또는 가공할 수 없습니다.

- 귀하는, 이 저작물의 재이용이나 배포의 경우, 이 저작물에 적용된 이용허락조건을 명확하게 나타내어야 합니다.
- 저작권자로부터 별도의 허가를 받으면 이러한 조건들은 적용되지 않습니다.

저작권법에 따른 이용자의 권리는 위의 내용에 의하여 영향을 받지 않습니다.

이것은 이용허락규약(Legal Code)을 이해하기 쉽게 요약한 것입니다.

Disclaimer

dCollection

약학석사학위논문

Chemical Constituents of the Seeds of *Aesculus turbinata* and Their PEDV Inhibitory Activity

칠엽수 열매로부터 얻은 화학성분과 PEDV 저해 활성 확인

2017 년 2 월

서울대학교 대학원

약학과 생약학 전공

김 지 원

Abstract

Porcine epidemic diarrhea virus (PEDV) causes severe diarrhea and high fatality of piglets, influencing the swine industry. Japanese horse chestnut (seed of *Aesculus turbinata*) contains many saponin mixtures, called escins, and has been used for a long time as a traditional medicinal plant. Structure-activity relationship (SAR) studies on escins have revealed that acylations at C-21 and C-22 with angeloyl or tigoloyl groups were important for their cytotoxic effects. However, the strong cytotoxicity of escins makes them hard to utilize for other diseases and to develop as nutraceuticals. In this research, we investigated whether escin derivatives **1**-**7** (including new compounds **2**, **3**, **5** and **6**), without the angeloyl or tigloyl groups and with modified glycosidic linkages by hydrolysis, have PEDV inhibitory effects with less cytotoxicity than the major compounds **8**-**10** isolated from the extract. Compounds **1**-**7** had no cytotoxicity at 20 μM on VERO cells, while compounds **8**-**10** showed strong cytotoxicity at similar concentrations, and also had moderate inhibitory activities on PEDV. Our results suggest that escin derivatives, which were prepared by two-step reactions, showed strong inhibitory activities on PEDV replication with less cytotoxicity. These studies proposed a method to utilize Japanese horse chestnut for treating PEDV with less cytotoxic effects, and to increase the diversity of its bioactive compounds.

Keywords: *Aesculus turbinata* Bl., Sapindaceae, escin, cytotoxicity, hydrolysis, oleanane-type triterpenoids, PEDV.

Student Number: 2015-21870

Table of contents

Abstract ..... **i**

List of Abbreviations ..... **v**

List of Figures ..... **vi**

List of Tables ..... **iix**

List of Schemes ..... **iix**

I. Introduction **1**

1. Coronaviruses 1

2. Porcine epidemic diarrhea virus 2

3. *Aesculus turbinata* Blume 2

II. Materials and Methods **4**

1. Plant materials 4

2. Reagents 4

3. Experimental instruments 5

4. Extraction, reaction and isolation schemes 6

4-1. Extraction of *A. turbinata* seeds, two-step hydrolysis, and fractionation 6

4-2. Chemical and spectral properties of isolated compounds 7

5. Bioassay procedures 16

5-1. Cell cultures and materials 16

5-2. I Cytotoxicity assay 16

5-3. Cytopathic effect (CPE) inhibition assay using PEDV 16

5-4. Quantitative real-time PCR 16

5-5. Western blot analysis 17

5-6. Immunocytochemistry assay.....17

5-7. Computer modelling of 3CL protease inhibition 18

5-8. Statistic analysis.....18

III. Results and Discussion 19

1. Structural elucidation of isolated compounds (**1**-**10**) 19

1-1. Compound **1**.....19

1-2. Compound **2**.....21

1-3. Compound **3**.....24

1-4. Compound **4**.....27

1-5. Compound **5**.....28

1-6. Compound **6**.....33

1-7. Compound **7**.....36

1-8. Compound **8**.....38

1-9. Compound **9**.....40

1-10. Compound **10**.....42

2. Cytotoxicity of fractions and isolated compounds.....46

3. PEDV inhibitory activities of fractions and isolated compounds 48

3-1. Evaluation of PEDV inhibitory activities by CPE assay 48

3-2. Evaluation of PEDV inhibitory activities by Western blot assay 51

3-3. Evaluation of PEDV inhibitory activities by real-time PCR 53

3-4. Evaluation of PEDV inhibitory activities by immunocytochemistry assay 55

3-5. Computer modelling of SARS-CoV 3CL protease inhibition 56

IV. Conclusions.....57

V. References 58

국문초록 62

List of Abbreviations

$3CL^{pro}$: 3C-Chymotrypsin-Like protease

ACN: Acetonitrile

$[\alpha]_{20}^{D}$: specific rotation at 20 Celsius degrees

BuOH: butanol

CC: Column chromatography

DMSO: dimethyl sulfoxide

d: doublet

dd: doublet of doublet

DMEM: Dulbecco's Modified Eagle's Medium

ESI-MS: ElectroSpray Ionization Mass Spectroscopy

EtOAc: ethyl acetate

EtOH: ethanol

fr.: fraction

HSQC: Heteronuclear Single Quantum Coherence

HMBC: Heteronuclear Multiple Bond Correlation

HPLC: High Performance Liquid Chromatography

HRESIMS: High Resolution ElectroSpray Ionization Mass Spectroscopy

Hz: Hertz

IR: infrared (spectrum)

MeOH: methanol

m/*z*: mass to charge ratio

NMR: nuclear magnetic resonance

ODS: octadecyl-bonded silica gel

PEDV: Porcine Epidemic Diarrhea Virus

ROESY: Rotating frame nuclear Overhauser Effect Spectroscopy

RP: reversed-phase (silica gel)

s: singlet

t: triplet

TLC: Thin-Layer Chromatography

UV: ultraviolet (spectrum, detector)

List of Figures

Figure 1. Illustration of Coronavirus structure 2
Figure 2. ^{1}H, ^{13}C NMR spectra of compound **1** 20
Figure 3. ^{1}H, ^{13}C NMR spectra of compound **2** 22
Figure 4. HMBC spectrum of compound **2** 23
Figure 5. ^{1}H, ^{13}C NMR spectra of compound **3** 25
Figure 6. HMBC spectrum of compound **3** 26
Figure 7. ^{1}H, ^{13}C NMR spectra of compound **4** 28
Figure 8. ^{1}H, ^{13}C NMR spectra of compound **5** 30
Figure 9. HMBC spectrum of compound **5** 31
Figure 10. ROESY spectrum of compound **5** 32
Figure 11. ^{1}H, ^{13}C NMR spectra of compound **6** 34
Figure 12. HMBC spectrum of compound **6** 35
Figure 13. ^{1}H, ^{13}C NMR spectra of compound **7** 37
Figure 14. ^{1}H, ^{13}C NMR spectra of compound **8** 39
Figure 15. ^{1}H, ^{13}C NMR spectra of compound **9** 41
Figure 16. ^{1}H, ^{13}C NMR spectra of compound **10** 43
Figure 17. Structures of compounds isolated from the seeds of *Aesculus turbinata* 44
Figure 18. Negative ESI-MS spectrum comparison between *n*-BuOH part from extract and reaction part from a two-step hydrolysis. 45
Figure 19. Cytotoxicity assay of fractions in 10 μg/mL 46
Figure 20. Cytotoxicity assay of compounds **1**-**10** at a concentration of 20 μM 47
Figure 21. Cytotoxicity assay of compounds **8**, **9** and **10** at concentrations of 2, 5 and 10 μM 47
Figure 22. CPE inhibition assay of *n*-BuOH fraction and reaction fraction in 1, 2, 5, and 10 μg/mL 49
Figure 23. Inhibitory effects of compounds **1**-**10** on PEDV replication in Vero cells 49

Figure 24. Inhibition of PEDV replication by compounds **4**-**6** at concentrations of 10, 20, and 40 μM 50
Figure 25. Inhibitory effects of compounds **1**, **4**, **5**, **6**, and **7** on PEDV nucleocapsid synthesis, using Western blot assay 51
Figure 26. Inhibitory effects of compound **4** on PEDV nucleocapsid and spike protein synthesis, using Western blot analysis.....52
Figure 27. Inhibitory activites of compounds **4** and **6** on PEDV RNA expression encoding nucleocapsid and spike protein estimated by RT-PCR at the concentration of 40 μM.....53
Figure 28. By RT-PCR analysis, compound **4** was analysed for its inhibitory on PEDV RNA expression encoding nucleocapsid and spike protein at the concentration of 10, 20 and 40 μM 54
Figure 29. Immunocytochemistry assay showed that PEDV replication was inhibited by compound **4** in dose-dependent manner.....55
Figure 30. Docking simulation of 3CL protease (PDB: 3V3M) with compound **4** and its interaction 56

List of Tables

Table 1. ^{13}C NMR data of new compounds **2**, **3**, **5**, and **6** in pyridine-d_5.....12

Table 2. ^{1}H NMR data of new compounds **2**, **3**, **5**, and **6** in pyridine-d_5 14

Table 3. Primers used for Real-time PCR.....54

List of Schemes

Scheme 1. Extraction, fractionation of the seeds of *A. turbinata* and isolation of fractions.....7

I. Introduction

1. Coronaviruses

Coronaviruses (CoVs) have been reported as the causes of different diseases at respiratory, enteric or central nervous system in many species including bats, pigs, horses and humans (Boheemen et al., 2012). These viruses are enveloped, single-stranded RNA viruses, constituting the largest RNA genomes in mammalian viruses, ranging from 25.5 to nearly 32 kb in length (Graham, Donaldson & Baric, 2013). Until 2003, only two coronaviruses were identified as infecting humans. However, severe acute respiratory syndrome coronavirus (SARS-CoV), was newly identified in 2002 to 2003, causing 10-50% mortality in infected individuals, affecting 27 countries, and exhibited atypical pneumonia (Boheemen, et al., 2012; Graham, Donaldson & Baric, 2013). A novel coronavirus, Middle East respiratory syndrome coronavirus (MERS-CoV), was first isolated and reported in Saudi Arabia, in 2012. The symptoms of MERS-CoV include acute pneumonia and severe renal failure in humans after infection (Zaki, Boheemen, Bestebroer, Osterhaus & Fouchier, 2012). This disease continued to emerge and spread to approximately 30 countries (Wit, Doremalen, Falzarano & Munster, 2016) and in May 2015, an outbreak of MERS occurred in South Korea via a traveller from the Middle East. Until the patient was diagnosed as infected with MERS-CoV, 29 secondary infections occurred by visiting different clinics, resulting in 186 confirmed cases (Wong, et al., 2015). At a molecular level, coronaviruses have important features such as high rates of RNA recombination, extraordinarily large RNA genomes and rapid stability after transmission to other species, leading to genetic diversity, unlike other enveloped RNA viruses (Masters, 2006).

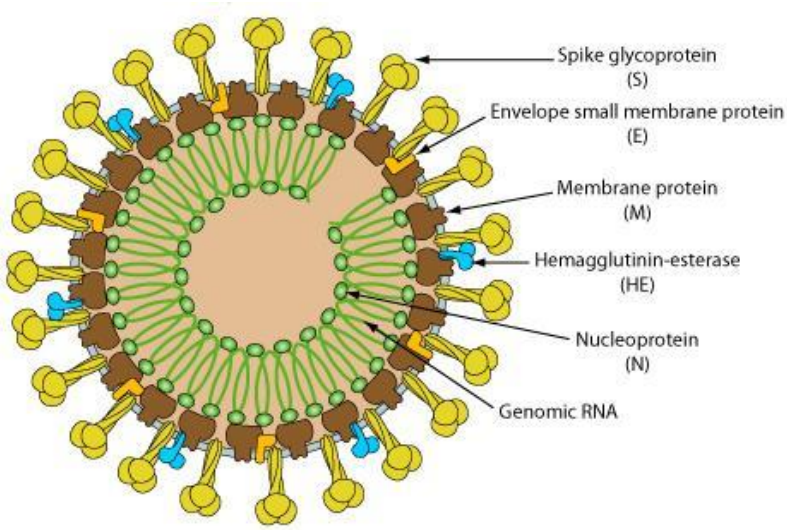


Figure 1. Illustration of Coronavirus structure

2. Porcine epidemic diarrhea virus (PEDV) and its purpose of study

PEDV, family *Coronaviridae*, genus *Alphacoronaviridae*, shares phylogenetically common features with other coronaviruses.[2] PEDV causes severe diarrhea, dehydration, vomiting in pigs of all ages, and high mortality of piglets, resulting in tremendous financial loss (Li, et al., 2013). Thus, these results imply the necessity of studying the characteristics of coronaviruses and discovering active drugs to prevent the fast and extensive spread of coronaviruses.

3. *Aesculus turbinata* Blume

Japanese horse chestnut *(Aesculus turbinata*) is a medicinal plant widely distributed in Korea, Japan and China (Yang, Zhao & Hattori, 2008). The seeds have been used for diverse biological activities including anti-inflammatory, anti-obese, hypoglycemic, and anti-cancer effects (Sato, Kofujita, Suzuki, Kobayashi & Tsuda, 2006; Yoshikawa, et al., 1996; Hu, et al., 2008; Wang, Ownby, Zhang, Yuan & Li, 2010; Piao, et al., 2014). However, the industrial utilization of escins for application to diseases and development as nutraceuticals are limited so far due to their strong nonspecific cytotoxic effects. In 2004, escins were also reported to possess a strong antiviral effect against SARS-CoV with an EC_{50} of 6.0 μM and a SI value of 2.5 (Wu, et al., 2004). These reports prompted us towards the development of safer escin derivatives with anti-CoV activities. Structure-activity

relationship (SAR) studies with escins suggested that acylation at C-21 and C-22 was necessary for the cytotoxic effects (Podolak, Galanty & Sobolewska, 2010; Chan, 2007; Chan, Zhao, Che & Mak, 2008; Mojzisova, et al., 2013; Rimmon, et al., 2013). Additionally, in oleanane-type structures, cytotoxicity can be enhanced with methylation at C-24 and free hydroxyl at C-16, and altered by the site of glycosides (Sun, Fang, Wang & Hu, 2006; Wang, Ownby, Zhang, Yuan & Li, 2010). Thus, alkaline and acid hydrolysis of escins were applied to detach acyl moieties at C-21 and C-22, and provide varieties of sugar moieties at C-3.

II. Materials and Methods

1. Plant materials

The seeds of *A. turbinata* were collected from Seoul in 2014 and authenticated by Prof. (W.K. Oh). A voucher specimen (SNU2014-006) is deposited in the herbarium of the College of Pharmacy, Seoul National University, Korea.

2. Reagents

2-1. Chemical reagents

- Hydrochloric acid (Daejung, Korea)
- HP-20 (Mitsubishi chemical corporation, Japan)
- Sodium hydroxide (Merck, Germany)
- Reversed-phased silica gel (Cosmosil 75C_{18}-PREP)
- TLC Silica gel 60 RP-18 F_{254S} (20 x 20 cm plate)
- TLC visualization reagent: 10% H_2SO_4 in EtOH
- All solvents used for extraction and isolation (*n*-hexane, EtOAc, EtOH, *n*-BuOH) were of analytical grade (Daejung Chemical & Metals Co. Ltd., Korea). Solvents used for HPLC chromatography (ACN, MeOH) were purchased from HoneyWell Burdick & Jackson®, USA.
- NMR solvent (pyridine-d_5) was purchased from Cambridge Isotope Laboratories, Inc., USA.

2-2. Bioassay reagents

- Vero cells (African green monkey kidney cell line; ATCC CCR-81) (ATCC, Manassas, VA, USA)
- Porcine epidemic diarrhea virus (PEDV) (Choong Ang Vaccine Laboratory, Korea)
- Dulbeccoʼs Modified Eagleʼs Medium (DMEM) (Hyclone, Logan, UT, USA)
- Fetal bovine serum (FBS) (Hyclone, Logan, UT, USA)
- FITC-conjugated goat anti-RbIgG antibody (Abcam, Cambridge, UK)
- Monoclonal antibody against N protein of PEDV (AbFrontier Co., Ltd., Seoul, Korea)
- Mounting reagent (Vectashield, Vector Laboratories Inc., Burlingame, CA, USA)

- Phosphate buffered saline (PBS) (Takara, Shiga, Japan)
- Peniciline (Sigma-Aldrich)
- Random primer (iNtRON Biotechnology, Seongman, Korea)
- Streptomycin (Sigma-Aldrich)
- 3-(4, 5-dimethyl-2-thiazolyl)-2,5-diphenyl-2*H*-tetrazolium bromide (MTT)
- Protein assay kit (Bio-Rad Laboratories, Hercules, CA, USA)
- Enhanced chemiluminescence Western blotting detection kit (Thermo Scientific, Rockford, IL, USA)

2-3. 3D modelling

- Discovery studio 4.0 (Accelrys, Sandiego, CA, USA)

3. Experimental instruments

- Analytical balance: Sartorius BSA 2245-CW (max 220 g, d= 0.1 mg), Germany.
- Autoclave: LAC-5080S, LAB Tech.
- Centrifuge (for filtration): AVANTI J2 BECKMAN COULTER®, USA.
  (for bioassay): FLETA S, Hanil Science Industrial Co.Ltd.
- Clean bench: Class II Biological Safety Cabinet, ESCO®.
- CO_2 incubator: Forma Series II water jacketed CO_2 incubator, THERMO.
- Drying oven: EYELA WFO-700, Japan.
- Evaporator: EYELA KSB-202, Japan.
- ESIMS spectrometer: Agilent, Q-TOF MS/Agilent, 1260 Infinity, USA.
- ESIMS/MS spectrometer: Agilent 6530 Q-TOF spectrometer (USA).
- Fraction collector: Waters Advantec 2120, USA.
- Fluorescence microscope: Olympus ix70 Fluorescence Microscope, Olympus Corporation, Japan.
- HPLC column: Reversed-phase C18 column (10 x 250 mm, 5 μm particle size, Cosmosil, Japan).
- HPLC system: Gilson 321 pump and Gilson UV/VIS 151 detector, USA.
- IR spectrometer: JASCO, FT/IR-4200, USA.
- NMR spectrometers
  - Agilent, Varian Gemini 2000, 300 MHz spectrometer, USA
  - Bruker AVANCE 400 spectrometer, Germany

- Bruker AVANCE 500 spectrometer, Germany
- Bruker AVANCE 800 HD spectrometer coupled with cryoprobe, Germany

- Polarimeter: JASCO P-2000 with a 10-mm cell, USA.
- Shaking incubator: BF-60SIR, BioFree®.
- Sonicator: Powersonic 420, Korea.
- StepOnePlus Real-Time PCR System, Applied Biosystems, Foster City, CA, USA.
- UV lamp: Vilber Lourmat VL-4.LC, France.
- Water purification system Direct-Q® & Direct-Q UV.
- Wise Therm heating mantle coupled with a feedback controller (WHM-C10A; DAIHAN Scientific Co., Ltd., Seoul, Korea)

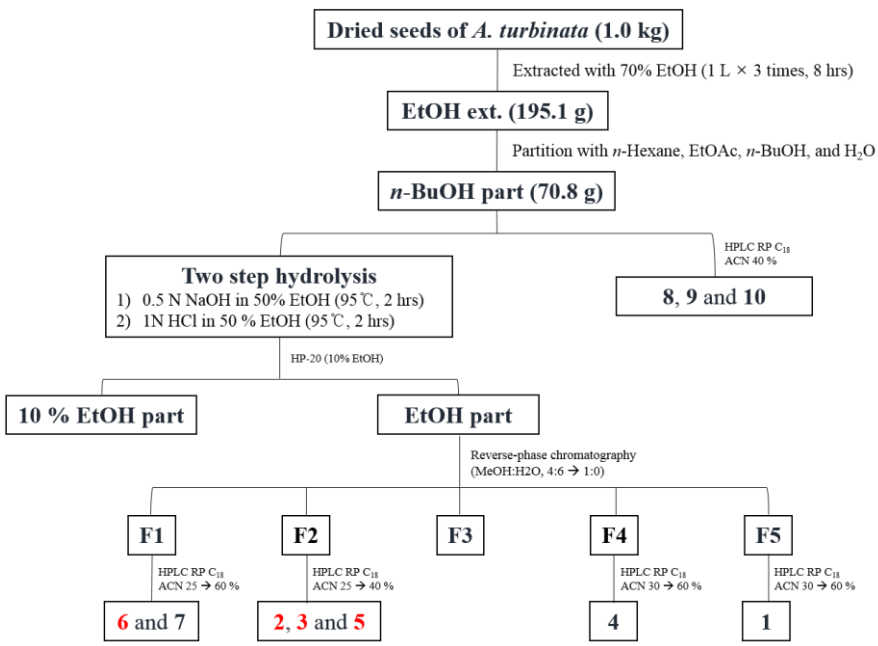
4. Extraction, reaction and isolation schemes

4-1. Extraction of *A. turbinata* seeds, two-step hydrolysis, and fractionation

The dried seeds of *A. turbinata* (1 kg) were extracted by sonication with 70% EtOH. The extract (195.1 g) was partitioned successively with *n*-hexane, EtOAc and *n*-BuOH. Since the *n*-BuOH-soluble fraction (70.8 g) contains a large amount of mixed triterpenoidal saponins called escins, this fraction was directly applied to hydrolysis reactions. These reactions proceeded in two steps. Acyl group hydrolysis was done at 100 ℃ in 0.5 N NaOH in 50% EtOH aqueous solution for 2 h. After neutralization, partial hydrolysis of the glucose moieties was also followed with 1.0 N HCl in 50% EtOH aqueous solution at 95 ℃ for 2 h. This reaction mixture was directly placed on an HP-20 CC (10 × 60 cm) to discard salt, washed with 10% EtOH (3 L), and finally eluted with EtOH (3 L) for the saponin fraction. The partial saponin fraction (15.59 g) was then chromatographed over a RP-C_{18} CC (40-63 μm particle size) and eluted with a gradient solvent system of MeOH:H_2O (from 4:6 to 1:0), to yield five fractions (F1-F5).

Fraction F1 was further applied to semi-preparative HPLC [RS Tech Optima Pak C18 column (250 × 10 mm, particle size 5 μm)]; (0-5 min: A:B (75:25), 5-24 min: A:B (75:25 to 40:60), 24-34 min: B; 0.1% formic acid in H_2O (A) and MeCN (B); flow rate 2 ml/min; UV detection at 205 and 254 nm) to isolate compounds **6** and **7**, respectively. Fraction F2 was also chromatographed by preparative HPLC (0-5 min; A:B (75:25), 5-25 min; A:B (75:25 to 60:40), 25-35 min; B) to provide

compounds **2**, **3** and **5**. Purification of fraction F4 by preparative HPLC (mobile phase MeCN/H_2O (30:70 to 60:40) over 25 min) resulted in the isolation of compound **4**. Fraction F5 was purified by preparative HPLC (mobile phase MeCN/H_2O (30:70 to 60:40) over 25 min) to provide compound **1**. Compound **8**, **9** and **10** were isolated from the *n*-BuOH fraction of the dried seeds of *A. turbinata* extract by semi-preparative HPLC using an isocratic solvent of 40% MeCN in 0.1% formic acid in H_2O over 40 min.



Scheme 1. Extraction, fractionation of the seeds of *A. turbinata* and isolation of fractions.

4-2. Chemical and spectral properties of isolated compounds

4-2-1. Compound **1**

White amorphous powder; $[\alpha]_{20}^{D}$ + 27.0 (*c*, 0.51, MeOH). UV λ_{max} (MeOH) (log ε) (nm) 195 (3.04); IR (KBr) ν_{max} 3400 cm^{-1}; ESIMS *m/z* 473.3 $[M+H-H_2O]^+$, 535.3 $[M+HCOO^-]^-$.

^{1}H NMR (300 MHz, pyridine-d_5): 5.46 (H-12, t-like s), 5.96 (16-OH, d; 4.5), 5.08 (16-H, overlap), 4.86 (H-21, d; 9.6), 4.70 (H-22, d; 9.6), 4.08 (28-CH_2, d; 10.5), 3.79 (28-CH_2, d; 10.2), 3.52 (H-3, dd; 6.0, 10.2), 3.13 (19-H, t; 13.8, 13.2),

2.89 (H-18, dd; 3.9, 14.1), 1.86 (CH_3-27), 1.42 (CH_3-30), 1.36 (CH_3-29), 1.25 (CH_3-23), 1.08 (CH_3-24), 0.98 (CH_3-25), 0.97 (CH_3-26).

^{13}C NMR (75 MHz, pyridine-d_5): 144.3 (C-13), 123.4 (C-12), 79.0 (C-21), 78.4 (C-3), 77.5 (C-22), 68.7 (C-28), 68.2 (C-16), 56.2 (C-5), 48.6 (C-19), 47.7 (C-17), 47.6 (C-9), 42.5 (C-14), 41.6 (C-18), 40.5 (C-8), 39.8. (C-4), 39.5 (C-1), 37.6 (C-10), 36.9 (C-20), 34.8 (C-15), 33.6 (C-7), 31.0 (C-29), 29.1 (C-23), 28.6 (C-2), 27.8 (C-27), 24.3 (C-11), 19.9 (C-30), 19.2 (C-6), 17.4 (C-26), 17.0 (C-24), 16.2 (C-25).

4-2-2. Compound **2**

Amorphous powder; $[\alpha]_{20}^{D}$ + 19.8 (*c* 0.1, MeOH); UV λ_{max} (MeOH) (log ε) (nm) 195 (3.50); IR (KBr) ν_{max} 3375, 2947, 2834, 1658, 1451, 1411, 1117, 1023 cm^{-1}; HRESIMS *m/z* 665.3901 (calcd for $C_{36}H_{57}O_{11}$ [M-H]$^-$, 665.3906); see Table 1 for ^{1}H (500 MHz, pyridine-d_5) and ^{13}C NMR (125 MHz, pyridine-d_5).

4-2-3. Compound **3**

Amorphous powder; $[\alpha]_{20}^{D}$ + 12.5 (*c* 0.1, MeOH); UV λ_{max} (MeOH) (log ε) (nm) 195 (3.51), 208 (3.38); IR (KBr) ν_{max} 3390, 2952, 2834, 1658, 1456, 1412, 1028 cm^{-1}; HRESIMS *m/z* 827.4434 (calcd for $C_{42}H_{67}O_{16}$ [M-H]$^-$, 827.4435); see Table 1 for ^{1}H (500 MHz, pyridine-d_5) and ^{13}C NMR (125 MHz, pyridine-d_5).

4-2-4. Compound **4**

White amorphous powder; $[\alpha]_{20}^{D}$ + 21.7 (*c* 0.2, pyridine); UV λ_{max} (MeOH) (log ε) (nm) 195 (3.11); IR (KBr) ν_{max} 3430, 2930, 2870, 1635, 1443, 1385, 1375, 1260, 1030, 703 cm^{-1}; ESIMS *m/z* 489.3 $[M+H-H_2O]^+$, 551.3 $[M+HCOO^-]^-$.

^{1}H NMR (300 MHz, pyridine-d_5): 5.97 (16-OH, d;4.8), 5.44 (H-12, t-like), 5.10 (H-16, overlap), 4.86 (H-21, d; 9.6), 4.70 (H-22, d; 9.6), 4.56 (24-CH_2, d; 11.1), 4.07 (28-CH_2, d; 10.2), 3.77 (24-CH_2, d; 10.5), 3.69 (28-CH_2, m), 3.66 (m), 3.12 (H-19, t-like dd; 13.8), 2.88 (H-18, dd; 3.6, 13.8), 1.87 (CH_3-27), 1.56 (CH_3-23), 1.42 (CH_3-30), 1.36 (CH_3-29), 0.94 (CH_3-25), 0.93 (CH_3-26).

^{13}C NMR (75 MHz, pyridine-d_5): 144.4 (C-13), 123.4 (C-12), 80.6 (C-3), 79.1 (C-21), 77.6 (C-22), 68.7 (C-28), 68.3 (C-16), 65.1 (C-24), 56.8 (C-5), 48.8 (C-19),

47.9 (C-9), 47.7 (C-17), 43.7 (C-4), 42.5 (C-14), 41.7 (C-18), 40.6 (C-8), 39.4 (C-1), 37.5 (C-10), 37.0 (C-20), 34.9 (C-15), 34.1 (C-7), 31.1 (C-29), 29.0 (C-2), 27.9 (C-27), 24.6 (C-11), 24.1 (C-23), 20.0 (C-30), 19.6 (C-6), 17.4 (C-26), 16.8 (C-25).

4-2-5. Compound **5**

Amorphous powder; $[\alpha]_{20}^{D}$ +32.7 (*c* 0.1, MeOH); UV λ_{max} (MeOH) (log ε) (nm) 195 (3.48), 215 (3.46), 285 (1.06); IR (KBr) ν_{max} 3385, 2952, 2834, 1657, 1456, 1412, 1028 cm^{-1}; HRESIMS *m/z* 681.3852 (calcd for $C_{36}H_{57}O_{12}$ $[M-H]^-$, 681.3856); see Table 1 for ^1H (800 MHz, pyridine-d_5) and ^{13}C NMR (200 MHz, pyridine-d_5).

4-2-6. Compound **6**

Amorphous powder; $[\alpha]_{20}^{D}$ +10.9 (*c* 0.1, MeOH); UV λ_{max} (MeOH) (log ε) (nm) 195 (3.23), 215 (3.01); IR (KBr) ν_{max} 3405, 2942, 1604, 1051, 1033 cm^{-1} ^{1}HRESIMS *m/z* 843.4384 (calcd for $C_{42}H_{67}O_{17}$ $[M-H]^-$, 843.4384); see Table 1 for ^1H (800 MHz, pyridine-d_5) and ^{13}C NMR (200 MHz, pyridine-d_5).

4-2-7. Compound **7**

Brown amorphous powder; $[\alpha]_{20}^{D}$ – 40.0 (*c* 2.04, pyridine); UV λ_{max} (MeOH) (log ε) (nm) 200(2.92), 210 (2.86); IR (KBr) ν_{max} 3388, 1724, 1630, 1060 cm^{-1}; ESIMS *m/z* 1005.5 $[M-H]^-$.

^1H NMR (300 MHz, pyridine-d_5): 5.66 (H-1′′, d; 7.8), 5.38 (H-12, br s), 5.25 (H-1′′′, d; 7.3), 5.03 (H-16, br s), 4.93 (H-1′, d; 7.4), 4.84 (H-21, d; 9.4), 4.67 (H-22, d; 9.5), 3.08 (H-19, t; 13.2), 2.83 (H-18, dd-like; 13.2), 1.85 (27-CH_3), 1.39 (23-CH_3), 1.34 (30-CH_3), 1.31 (29-CH_3), 0.84 (26-CH_3), 0.66 (25-CH_3).

^{13}C NMR (75 MHz, pyridine-d_5): 172.8 (C-6′), 144.2 (C-13), 123.1 (C-12), 104.9 (C-1′), 104.5 (C-1′′ and C-1′′′), 91.4 (C-3), 82.3 (C-4′), 79.9 (C-2′), 79.0 (C-21), 78.8 (C-5′′′), 78.6 (C-5′′), 78.4 (C-3′′), 78.3 (C-3′′′), 77.4 (C-22), 76.8 (C-3′), 76.0 (C-5′), 75.2 (C-2′′), 74.1 (C-2′′′), 71.8 (C-4′′′), 70.0 (C-4′′), 68.4 (C-28), 68.1 (C-16), 63.6 (C-24), 62.7 (C-6′′′), 62.0 (C-6′′), 56.4 (C-5), 48.5 (C-19), 47.7 (C-17), 47.1 (C-9), 44.0 (C-4), 42.3 (C-14), 41.3 (C-18), 40.2 (C-8), 38.8 (C-1), 36.8 (C-

10), 36.7 (C-20), 34.6 (C-15), 33.5 (C-7), 30.9 (C-29), 27.7 (C-27), 26.9 (C-2), 24.4 (C-11), 22.8 (C-23), 19.8 (C-30), 18.8 (C-6), 17.0 (C-26), 15.9 (C-25).

4-2-8. Compound **8**

Brown amorphous powder; $[\alpha]_{20}^{D}$ – 22.5 (*c* 0.6, MeOH); UV λ_{max} (MeOH) (log ε) (nm) 200 (3.48), 220 (3.49); IR (KBr) ν_{max} 3453, 1731, 1719, 1653, 1649, 1638, 1075 cm^{-1}; ESIMS *m/z* 1153.4 $[M+Na]^+$, 1129.3 $[M-H]^-$.

^{1}H NMR (300 MHz, pyridine-d_5): 7.12 (Tig-H-1‴, d; 7.1), 6.61 (H-21, d; 9.9), 6.28 (H-22, d; 10.1), 5.65 (H-1″, d; 7.5), 5.37 (H-12, br s), 5.21 (H-1‴, d-like), 4.92 (H-1′, d; 6.8), 3.07 (H-18, br s), 1.95 (Ac-2⁗-CH_3, s), 1.89 (Tig-5‴-CH_3, s), 1.65 (Tig-4‴-CH_3, d; 7.0) 1.81 (27-CH_3), 1.32 (23-CH_3, 30-CH_3), 1.09 (29-CH_3), 0.79 (26-CH_3), 0.63 (25-CH_3).

^{13}C NMR (75 MHz, pyridine-d_5): 171.0 (C-1⁗), 168.0 (C-1‴), 142.9 (C-13), 136.8 (C-3‴), 129.5 (C-2‴), 122.8 (C-12), 104.7 (C-1‴), 104.6 (C-1′), 104.2 (C-1″), 91.1 (C-3), 79.6 (C-2′), 79.3 (C-21), 78.5 (C-5‴), 78.3 (C-5″), 78.1 (C-3‴), 78.0 (C-3″), 76.5 (C-3′), 75.7 (C-5′), 74.3 (C-22), 71.4 (C-4‴), 68.0 (C-16), 63.7 (C-28), 63.3 (C-24), 62.3 (C-6‴), 61.5 (C-6″), 56.3 (C-5), 47.9 (C-17), 47.2 (C-19), 46.7 (C-9), 43.6 (C-4), 41.6 (C-14), 40.0 (C-18), 39.9 (C-8), 38.4 (C-1), 36.4 (C-10), 36.3 (C-20), 34.6 (C-15), 33.2 (C-7), 29.5 (C-29), 27.4 (C-27), 26.5 (C-2), 24.0 (C-11), 22.4 (C-23), 20.9 (C-2⁗), 20.1 (C-30), 18.5 (C-6), 16.7 (C-26), 15.5 (C-25), 14.2 (C-4‴), 12.4 (C-5‴).

4-2-9. Compound **9**

Brown amorphous powder; $[\alpha]_{20}^{D}$ – 23.1 (*c* 0.6, MeOH); UV λ_{max} (MeOH) (log ε) (nm) 195 (3.49), 220 (3.47); IR (KBr) ν_{max} 3432, 1731, 1719, 1653, 1649, 1638, 1075 cm^{-1}; ESIMS *m/z* 1153.5 $[M+Na]^+$, 1129.3 $[M-H]^-$.

^{1}H NMR (500 MHz, pyridine-d_5): 6.62 (H-21, d; 9.9), 6.22 (H-22, d; 9.9), 5.98 (Ang-H‴-3, dq; 7.2), 5.60 (H-1″, d-like), 5.46 (H-12, br s), 5.21 (H-1‴, d-like), 4.84 (H-1′), 4.30 (24-CH_2, overlap), 3.60 (28-CH_2, overlap), 3.36 (24-CH_2 and 28-CH_2, overlap), 3.06 (H-18, m), 2.11 (Ang-4‴-CH_3, d; 7.0), 2.02 (Ac-2⁗-

CH_3, s), 1.92 (Tig-5′′′′-CH_3, s), 1.82 (27-CH_3), 1.32 (30-CH_3), 1.30 (23-CH_3, 29-CH_3), 1.08 (26-CH_3), 0.79 (25-CH_3).

^{13}C NMR (125 MHz, pyridine-d_5): 170.7 (C-1′′′′), 168.2 (C-1′′′), 143.2 (C-13), 137.5 (C-3′′′), 129.5 (C-2′′′), 123.4 (C-12), 105.2 (C-1′′′), 104.9 (C-1′), 104.6 (C-1′′), 91.5 (C-3), 79.8 (C-2′), 79.7 (C-21), 79.2 (C-5′′′), 78.8 (C-5′′), 78.4 (C-3′′′), 78.1 (C-3′′), 77.0 (C-3′), 76.0 (C-5′, C-2′′), 75.2 (C-2′′′), 74.6 (C-22), 71.6 (C-4′′′), 68.3 (C-16), 64.1 (C-28), 63.6 (C-24), 62.6 (C-6′′′), 62.0 (C-6′′), 56.4 (C-5), 48.3 (C-17), 47.5 (C-19), 47.0 (C-9), 44.0 (C-4), 42.0 (C-14), 41.3 (C-18), 40.2 (C-8), 38.9 (C-1), 36.8 (C-10), 36.6 (C-20), 35.0 (C-15), 33.5 (C-7), 29.8 (C-29), 27.7 (C-27), 26.8 (C-2), 24.4 (C-11), 22.8 (C-23), 21.3 (C-5′′′), 20.8 (C-2′′′′), 20.6 (C-30), 18.8 (C-6), 17.0 (C-26), 16.0 (C-25), 14.2 (C-4′′′)

4-2-10. Compound **10**

Brown amorphous powder; $[\alpha]_{20}^{D}$ – 12.0 (*c* 0.13, MeOH); UV λ_{max} (MeOH) (log ε) (nm) 200 (3.48), 210 (3.47); IR (KBr) ν_{max} 3416, 2926, 1723, 1686, 1268, 1079 cm^{-1}; ESIMS *m/z* 1153.4 $[M+Na]^+$, 1129.4 $[M-H]^-$.

^{1}H NMR (500 MHz, pyridine-d_5): 7.02 (Tig-H-1′′′′, d; 6.4), 6.46 (H-21, d; 9.8), 5.60 (H-1′′, d; 7.2), 5.44 (H-12, br s), 5.22 (H-1′′′, d; 7.5), 4.89 (H-1′, d; 7.4), 4.75 (H-16, br s), 2.86 (H-18, dd; 13.6, 3.4), 2.02 (Ac-2′′′′-CH_3), 1.85 (Tig-5′′′′-CH_3, s), 1.81 (27-CH_3), 1.60 (Tig-2′′′′-CH_3, d; 7.1), 1.31 (23-CH_3, 30-CH_3), 1.10 (29-CH_3), 0.92 (26-CH_3), 0.65 (25-CH_3).

^{13}C NMR (125 MHz, pyridine-d_5): 171.0 (C-1′′′′), 168.8 (C-1′′′), 143.0 (C-13), 136.6 (C-3′′′), 130.1 (C-2′′′), 123.4 (C-12), 105.0 (C-1′, C-1′′′), 104.6 (C-1′′), 91.4 (C-3), 81.9 (C-4′), 81.3 (C-21), 80.0 (C-2′), 78.8 (C-5′′′), 78.6 (C-5′′), 78.4 (C-3′′′), 78.3 (C-3′′), 76.8 (C-3′), 76.0 (C-5′, C-2′′), 75.2 (C-2′′′), 71.8 (C-4′′′), 71.5 (C-22), 70.1 (C-4′′), 67.9 (C-16), 66.7 (C-28), 63.6 (C-24), 62.6 (C-6′′′), 61.9 (C-6′′), 56.4 (C-5), 47.6 (C-19), 47.4 (C-17), 47.0 (C-9), 44.0 (C-4), 42.1 (C-14), 40.9 (C-18), 40.2 (C-8), 38.8 (C-1), 36.6 (C-10, C-20), 34.9 (C-15), 33.5 (C-7), 29.8 (C-29), 27.7 (C-27), 26.8 (C-2), 24.4 (C-11), 22.8 (C-23), 21.0 (C-2′′′′), 20.4 (C-30), 18.8 (C-6), 17.2 (C-26), 15.9 (C-25), 14.4 (C-4′′′), 12.7 (C-5′′′).

Table 1. ^{13}C NMR data of new compounds **2**, **3**, **5**, and **6** in pyridine-d_5 (δ in ppm)

Position	**2**[a]	**3**[a]	**5**[b]	**6**[b]
1	39.0	39.0	38.9	38.9
2	26.8	26.8	27.2	27.1
3	89.1	89.2	89.2	89.3
4	39.7	39.7	44.7	44.7
5	56.0	55.9	56.4	56.4
6	18.6	18.6	19.1	19.1
7	33.4	33.3	33.7	33.7
8	40.2	40.2	40.3	40.3
9	47.2	47.2	47.2	47.2
10	37.0	37.0	36.8	36.8
11	24.0	24.0	24.4	24.4
12	123.2	123.1	123.2	123.3
13	144.1	144.1	144.2	144.3
14	42.2	42.2	42.3	42.4
15	34.5	34.5	34.6	34.6
16	68.0	68.0	68.2	68.2
17	47.5	47.5	47.7	47.7
18	41.3	41.3	41.3	41.5
19	48.4	48.4	48.5	48.5
20	36.6	36.6	36.7	36.8
21	78.9	78.8	79.0	79.0
22	77.5	77.4	77.5	77.5
23	28.3	28.3	23.6	23.6
24	17.2	17.1	63.6	63.5
25	16.0	15.9	15.8	15.8
26	17.1	17.1	17.1	17.2
27	27.6	27.6	27.7	27.7
28	68.6	68.5	68.5	68.6
29	30.8	30.7	30.9	30.9
30	19.6	19.6	19.8	19.8
GlcA				
1′	107.4	107.0	106.7	106.2
2′	75.7	75.1	75.7	75.2
3′	78.4	76.1	78.4	76.9
4′	73.7	82.9	73.9	83.9
5′	77.9	76.6	78.3	76.9

6′	n.d	n.d	173.4	n.d
Glc				
1″		105.0		105.3
2″		75.0		75.4
3″		78.2		78.4
4″		71.7		72.0
5″		78.6		78.8
6″		62.7		62.9

ppm, [a] Recorded in 125 MHz. [b] Recorded in 200 MHz.

Table 2. ^{1}H NMR data of new compounds **2**, **3**, **5**, and **6** in pyridine-d_5 (δ in ppm)

Position	**2**[a]	**3**[a]	**5**[b]	**6**[b]
1	1.47, 0.94	1.45, 0.90	1.46, 0.91	1.43, 0.85
2	1.92, 1.76	2.24 (d-like; 11.1), 1.85	2.23 (d-like; 10.2), 2.03 (d-like)	2.17 (d-like; 12.9), 2.00 (dd-like; 11.0)
3	3.42 (dd-like)	3.41 (dd-like)	3.63 (dd-like; 11.8)	3.56 (d; 10.8)
5	0.80	0.82	0.94 (d; 11.5)	0.91 (d; 12.3)
6	1.61, 1.50	1.65, 1.51	1.65, 1.36	1.62, 1.35
7	1.62, 1.32	1.63, 1.31 (overlap)	1.59, 1.31	1.59, 1.30
9	1.77	1.77	1.76	1.74 (m)
11	1.92, 1.79	1.93, 1.87	1.91, 1.80	1.91, 1.79
12	5.39 (br s)	5.42 (br s)	5.38 (br s)	5.39 (br s)
15	2.10 (d; 12.3), 1.69 (d; 14.3)	2.12 (d; 11.8), 1.71 (d; 14.2)	2.08 (dd-like; 14.5, 3.5), 1.69 (d; 13.5)	2.08 (d-like; 11.2), 1.68 (d; 13.8)
16	5.03 (overlap)	5.04 (overlap)	5.02 (br s)	5.02 (br s)
18	2.80 (dd-like; 13.0)	2.82 (dd-like)	2.80 (dd; 14.0, 3.7)	2.81 (dd; 13.3, 3.7)
19	3.06 (t; 13.4), 1.43	3.08 (t; 13.5)	3.02 (t; 13.5), 1.42 (dd; 12.9, 4.2)	3.05 (t; 13.4), 1.42 (d-like)
21	4.80 (d; 8.6)	4.82 (d; 9.5)	4.80 (d; 9.6)	4.81 (d; 9.4)
22	4.63 (d-like; overlap)	4.65 (d; 9.6)	4.64 (d; 9.5)	4.64 (d; 9.5)
23	1.30	1.31	1.53	1.49
24	1.00	1.02	4.40 (d; 11.2), 3.65 (d; 11.4)	4.37 (d; 11.0), 3.62 (d; 10.6)
25	0.85	0.87	0.80	0.78
26	0.90	0.92	0.88	0.88
27	1.88	1.90	1.88	1.89
28	4.02 (d; 10.3), 3.72 (dd; 10.1)	4.04 (d; 10.6), 3.74 (overlap)	4.00 (d; 10.5), 3.71 (d; 10.3)	4.10 (d; 10.3), 3.72 (d; 10.4)
29	1.32	1,35	1.33	1.33
30	1.38	1.43	1.40	1.39
GlcA				
1′	5.03 (overlap)	5.03 (overlap)	5.18 (d; 7.4)	5.09 (overlap)

2′	4.13 (t-like)	4.15 (t-like)	4.12 (t; 8.2)	4.11 (overlap)
3′	4.32 (t-like)	4.37 (t; 7.5)	4.35 (t; 8.8)	4.32 (t; 7.2)
4′	4.58 (overlap)	4.61 (overlap)	4.60 (t-like)	4.54 (overlap)
5′	4.67 (overlap)	4.75 (d; 7.8)	4.73 (d-like)	4.69
Glc				
1″		5.25 (d; 6.4)		5.22 (overlap)
2″		4.09 (t; 8.0)		4.07 (t; 7.3)
3″		4.23 (overlap)		4.25 (overlap)
4″		4.15 (overlap)		4.12 (overlap)
5″		4.02 (overlap)		4.00 (overlap)
6″		4.53 (d; 11.0), 4.27 (overlap)		4.52, 4.23 (both overlap)

ppm, *J* in Hz. [a] Recorded in 500 MHz. [b] Recorded in 800 MHz.

5. Bioassay procedures

5-1. Cell culture and virus stock

Vero cells (African green monkey kidney cell line; ATCC CCR-81) were obtained from American Type Culture Collection (ATCC, Manassas, VA, USA). Cells were grown in Dulbecco's Modified Eagle's Medium (DMEM) supplemented with 100 U/mL penicillin, 100 μg/mL streptomycin and 10% fetal bovine serum (FBS). PEDV was provided by Choong Ang Vaccine Laboratory, Korea. Virus stock was maintained at -80℃ before use.

5-2. Cytotoxicity assay

To assess the cell viability, a MTT (3-(4,5-dimethyl-2-thiazolyl)-2,5-diphenyl-2*H*-tetrazolium bromide) assay was carried out. Vero cells were seeded for 24 h in 96-well plates at 1×10^5 cells per well. Then, the cells were exposed to different concentrations of fractions and compounds for 48 h. The final concentration of DMSO was maintained at 0.05% (v/v) to avoid solvent toxicity. 20 μL of MTT solution (2 mg/mL) was then added to cultures and incubated for 4 h. Formazan crystals were dissolved with 100 μL of DMSO, and the optimal densities (OD) were measured at 550 nm.

5-3. Cytopathic effect (CPE) inhibition assay using PEDV

Vero cells were grown in 96-well plates at 1×10^5 cells per well. After 24 h, the medium was removed and washed with phosphate buffered saline (PBS). PEDV (0.01 MOI) were inoculated onto confluent monolayers of Vero cells for 2 h. The media were replaced by DMEM with different concentrations of compounds. After 72 h of incubation at 37℃ in a 5% CO_2-balanced air incubator, cells were replaced with DMEM. Then, 20 μL of MTT solution (2 mg/mL) was added to each well and incubated for 4 h.

5-4. Quantitative real-time PCR

Quantitative real-time PCR was performed using the StepOnePlus Real-Time PCR System (Applied Biosystems, Foster City, CA, USA). Vero cells were seeded at 90% confluence in 6-well plates, infected with PEDV (0.01 MOI), and incubated for 2 h. Then the medium was replaced by DMEM and cultured with different

concentrations of compounds. After 24 h, total RNA from the cells was isolated by TRIzol method and reverse transcribed using random primer (iNtRON Biotechnology, Seongman, Korea) according to the manufacturer' protocol. Amplifications were carried out using selective primers for PEDV, which are listed in S-Table 1 (Supporting Information), using 2 μL of cDNA and Maxima SYBR Green qPCR master mix 2X (Thermo Scientific, Rockford, IL, USA). Cyclic conditions were as follows: initial denaturation at 95℃ for 10 min, 40 cycles with 95℃ for 15 s and 60℃ for 1 min.

5-5. Western blot analysis

Whole-cell lysates were prepared by scraping adherent-cultured cells with 100 μL of lysis buffer (0.5% NP-40, 50 mM NaF, 1 mM EDTA, 120 mM NaCl, 50 mM Tris-HCl (pH 7.6)) and centrifuged at 12,000 rpm for 20 min. Protein concentrations of the supernatant were calculated using a protein assay kit (Bio-Rad Laboratories, Hercules, CA, USA). Aliquots of lysates were separated by 10-12% SDS-PAGE and electrophoretically transferred to PVDF membranes (PVDF 0.45 μm. Immobilon-P, USA). Membranes were incubated overnight with antibodies against spike (S) protein, nucleocapsid (N) (AbFrontier Co., Ltd., Seoul, Korea) or mouse monoclonal actin, and further incubated with secondary antibodies. Protein bands were detected using an enhanced chemiluminescence Western blotting detection kit (Thermo Scientific).

5-6. Immunocytochemistry assay

Cells were grown on sterilized glasses slides, and PEDV (0.01 MOI) was inoculated to the cell monolayers for 2 h. The solution was replaced with DMEM, treated with compounds for 24 h, washed in PBS (pH 7.4) and fixed with a 4% paraformaldehyde solution for 30 min at room temperature. The slides were blocked with 1% BSA for 1 h, and incubated with monoclonal antibody against N protein of PEDV (AbFrontier Co., Ltd., Seoul, Korea) diluted 1:50 with PBS (pH 7.4) for 24 hr. The slides were washed with PBS, and incubated with FITC-conjugated goat anti-RbIgG antibody (Abcam, Cambridge, UK) for 1 hr. After washing three times with PBS (pH 7.4), the slides were stained with 500 nM DAPI solution for 10 min at room temperature and washed with PBS (pH 8.0) three times.

Mounting reagent (Vectashield, Vector Laboratories Inc., Burlingame, CA, USA) was used. The slides were examined under a fluorescence microscope (Olympus ix70 Fluorescence Microscope, Olympus Corporation, Tokyo, Japan).

5-7. Computer modelling of 3CL protease inhibition

To understand the mechanism of isolated compounds acting as PEDV inhibitors, a molecular docking study was performed using the Discovery Studio 4.0/CDOCKER (Accelrys, Inc). The crystal structure of 0EM/3CL protease complex (PDB ID: 3V3M) was supplied from the Protein Data Bank (PDB) (Jacobs, et al., 2013).

5-8. Statistic analysis

All experiments were performed three times in duplicate and the data are presented as the mean ± SD. Statistical analysis was done with the unpaired student's *t*-test using Sigma Plot Statistical Analysis software. Statistical significance was accepted at $p < 0.05$.

III. Results and Discussion

1. Structural elucidation of isolated compounds (1-10)

1-1. Compound **1**

Compound **1** was obtained as white amorphous powder with $[\alpha]_{20}^{D}$ + 27.0 (*c*, 0.51, MeOH). IR spectral analysis showed the presence of hydroxyl (3400 cm^{-1}).

^{1}H NMR data indicated seven tertiary methyl groups at 1.86 (CH_3-27), 1.42 (CH_3-30), 1.36 (CH_3-29), 1.25 (CH_3-23), 1.08 (CH_3-24), 0.98 (CH_3-25), 0.97 (CH_3-26) along with olefinic proton at 5.46 (H-12) and several hydroxyl groups. ^{13}C NMR spectrum showed two olefinic carbon signals at δ_C 123.4 (C-12) and 144.3 (C-13), suggesting the structure as an oleanane-type triterpenoid.

Spectral data of **1** were observed to be identical to those of escinidin (Konoshima & Lee, 1986). Therefore, its structure was fully elucidated.

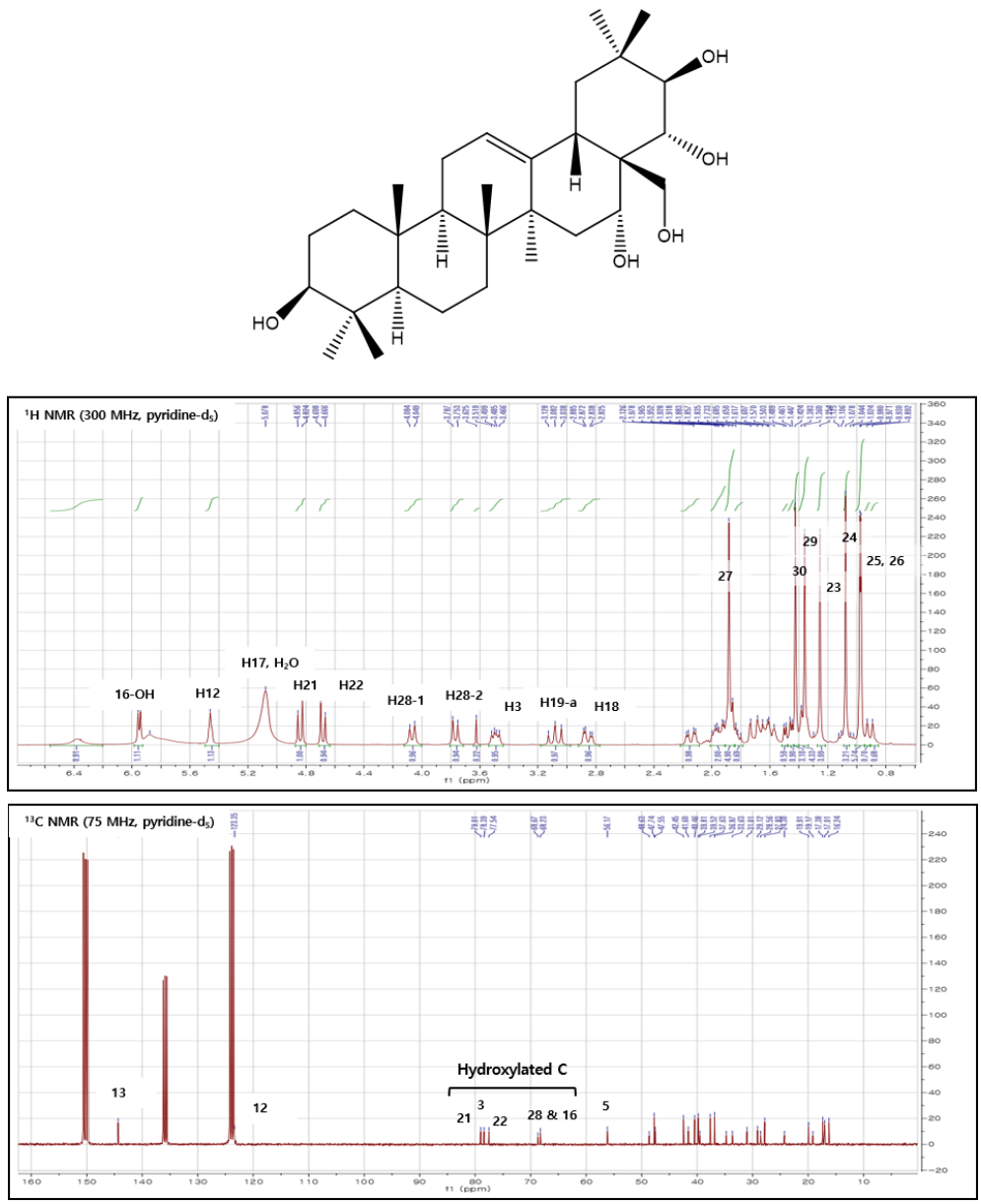


Figure 2. ^{1}H, ^{13}C NMR spectra of compound **1**

1-2. Compound **2**

Compound **2** was obtained as a brownish amorphous powder. Positive HRESIMS showed $[(M+H)+[-H_2O]]^+$ ion at *m/z* 649.3946 (calcd for 649.3946) and $[M-H]^-$ ion at *m/z* 665.3901 (calcd for 665.3906), deducing the molecular formula $C_{36}H_{58}O_{11}$. IR spectrum showed absorption due to hydroxyl (3375 cm^{-1}), olefinic bond (1658 cm^{-1}), and glycosidic linkage (1023 cm^{-1}). ^1H and ^{13}C NMR data of **2** proposed the structure as an olean-12-ene triterpenoid glucopyranosiduronic acid, exhibiting signals for seven tertiary methyl groups [δ_H 0.85 (CH_3-25), 0.90 (CH_3-26), 1.00 (CH_3-24), 1.30 (CH_3-23), 1.32 (CH_3-29), 1.38 (CH_3-30) and 1.88 (CH_3-27)], an olefinic proton at δ_H 5.39 (br s) with two olefinic carbon signals at δ_C 123.0 (C-12) and 144.0 (C-13), and one β-D-glucopyranosiduronic acid moiety [one anomeric proton at δ_H 5.03 (H-1′), along with five carbon signals at δ_C 107.2 (C-1′), 78.2 (C-3′), 77.7 (C-5′), 75.5 (C-2′) and 73.5 (C-4′)]. ^1H and ^{13}C NMR data of **2** was consistent with those of escinidin (**1**), except for the chemical shift of C-3 and the presence of one β-D-glucopyranosiduronic acid moiety in **2**. These results indicated the attachment of β-D-glucopyranosiduronic acid to C-3 (δ_C 89.0), while the chemical shift of C-3 in escinidin (**1**) only appeared at δ_C 78.0 (CH). Linkage position of this β-D-glucopyranosiduronic acid was confirmed by the HMBC experiment from the correlation from H-1′ (δ_H 5.03) to C-3 (δ_C 89.1). Therefore, the structure of **2** was elucidated as (3β,16α,21β,22α)-16,21,22,28-tetrahydroxyolean-12-en-3-O-β-D-glucopyranosiduronic acid.

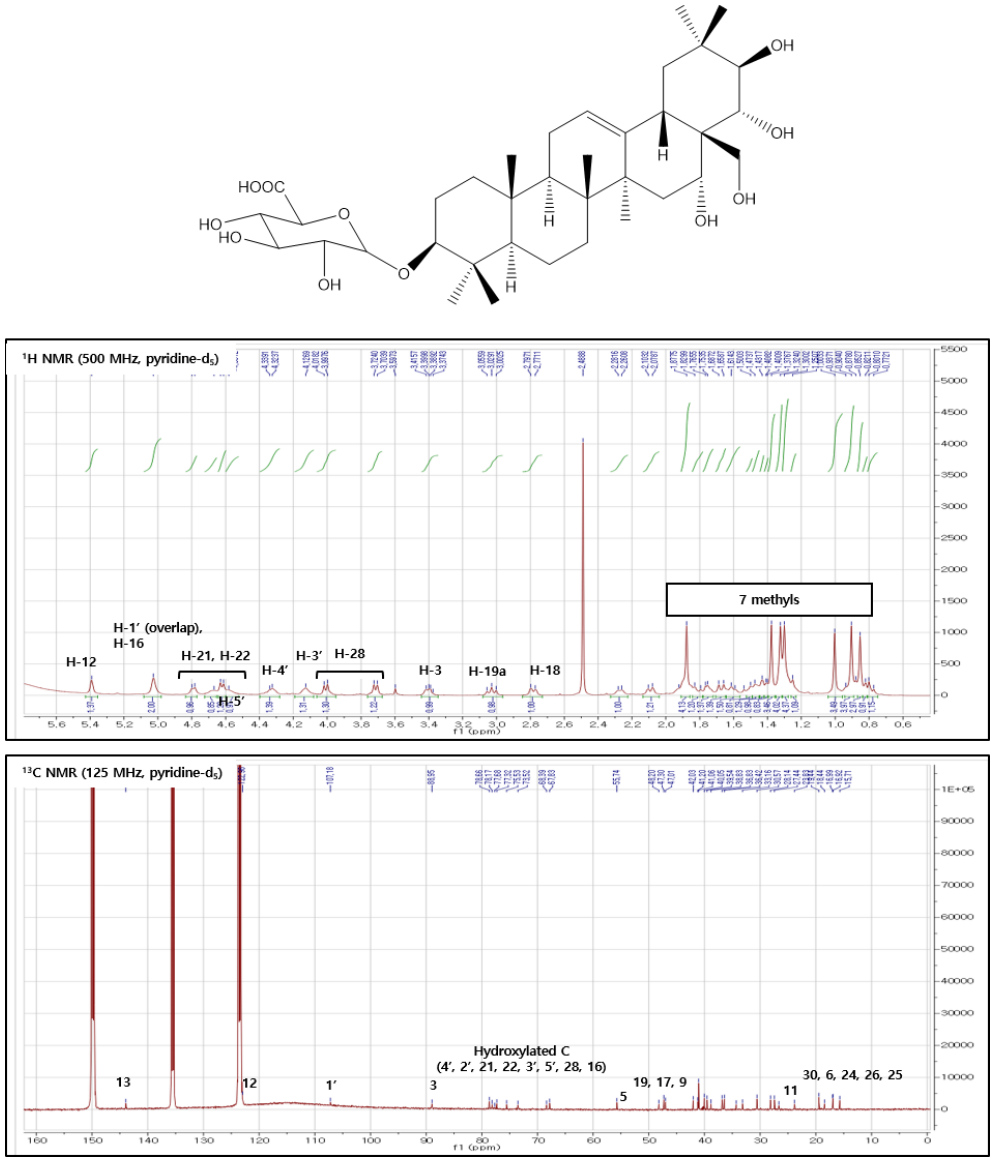


Figure 3. ^{1}H, ^{13}C NMR spectra of compound **2**

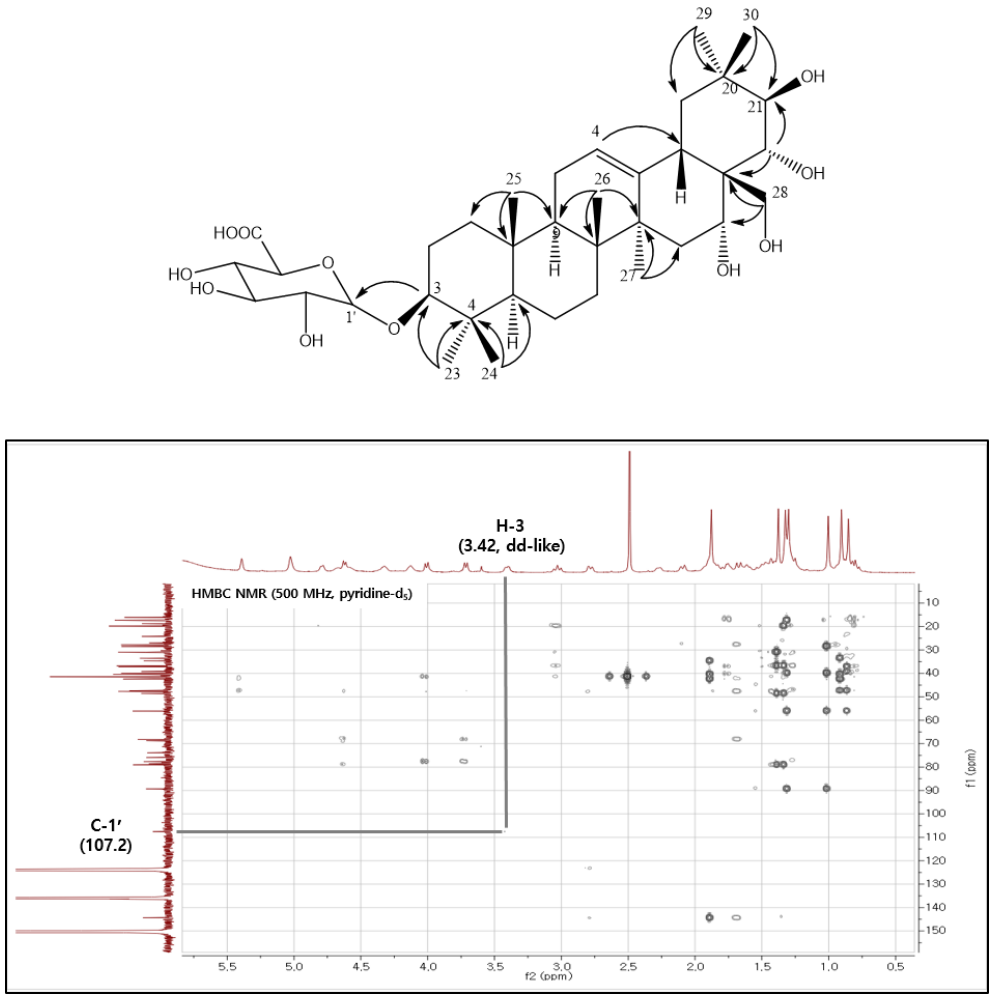


Figure 4. HMBC spectrum of compound **2**

1-3. Compound **3**

Compound **3** was isolated as a brownish amorphous powder, with the molecular formula $C_{42}H_{68}O_{16}$, as implied from the HRESIMS at *m/z* 851.4408 $[M+Na]^+$ (calcd for $C_{42}H_{68}O_{16}Na^+$, 851.4400) and at *m/z* 827.4434 $[M-H]^-$ (calcd for $C_{42}H_{67}O_{16}^-$, 827.4435). IR spectrum suggested the presence of hydroxyl (3390 cm^{-1}), olefinic bond (1658 cm^{-1}), and glycosidic linkage (1028 cm^{-1}). ^1H NMR spectrum showed signals for seven tertiary methyl groups [δ_H 0.87 (CH_3-25), 0.92 (CH_3-26), 1.02 (CH_3-24), 1.31 (CH_3-23), 1.35 (CH_3-29), 1.43 (CH_3-30) and 1.90 (CH_3-27)], an olefinic proton at δ_H 5.42 (br s) and two anomeric protons at δ_H 5.25 (1H, d, J = 6.4 Hz, H-1″) and 5.03 (1H, d-like, overlap, H-1′). ^{13}C NMR spectrum of **3** was very similar with those of **2**, apart from the presence of one *β*-D-glycopyranosyl moiety in **3**. Linkage position of the *β*-D-glycopyranosyl was identified by HMBC experiment. HMBC correlation between H-3 (δ_H 3.41) and C-1′ (δ_C 107.0) of the *β*-D-glucopyranosiduronic acid, H-4′ (δ_H 4.61) of the *β*-D-glucopyranosiduronic acid and C-1″ (δ_C 105.0) of the *β*-D-glycopyranosyl were observed, indicating that *β*-D-glucopyranosiduronic acid was attached to the carbon C-3 like **2**, and the other *β*-D-glycopyranosyl was linked at the C-4′ of *β*-D-glucopyranosiduronic acid. Thus, the structure of **3** was established as (3*β*,16*α*,21*β*,22*α*)-16,21,22,28-tetrahydroxyolean-12-en-3-yl-O-[*β*-D-glycopyranosyl-(1→4)]-*β*-D-glucopyranosiduronic acid.

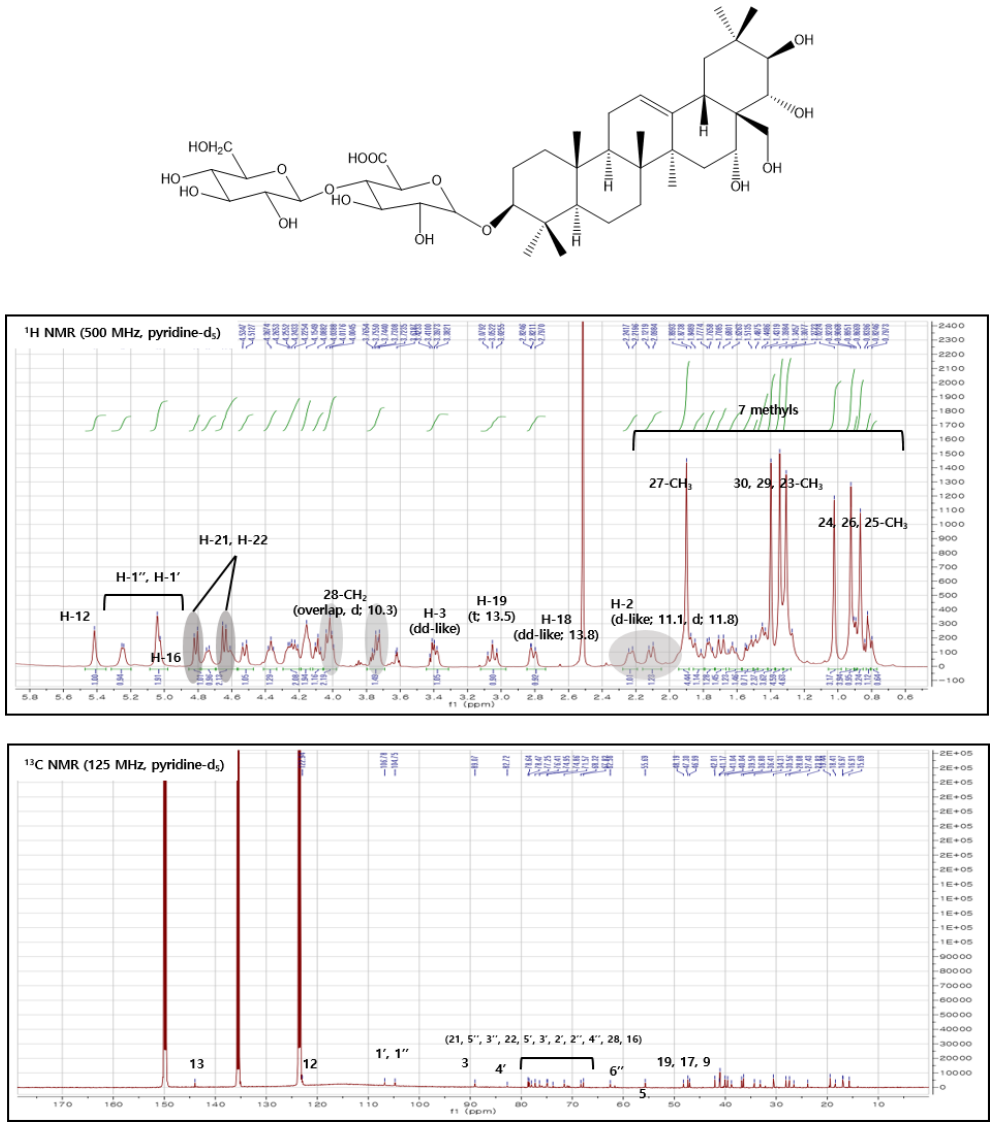


Figure 5. ^{1}H, ^{13}C NMR spectra of compound **3**

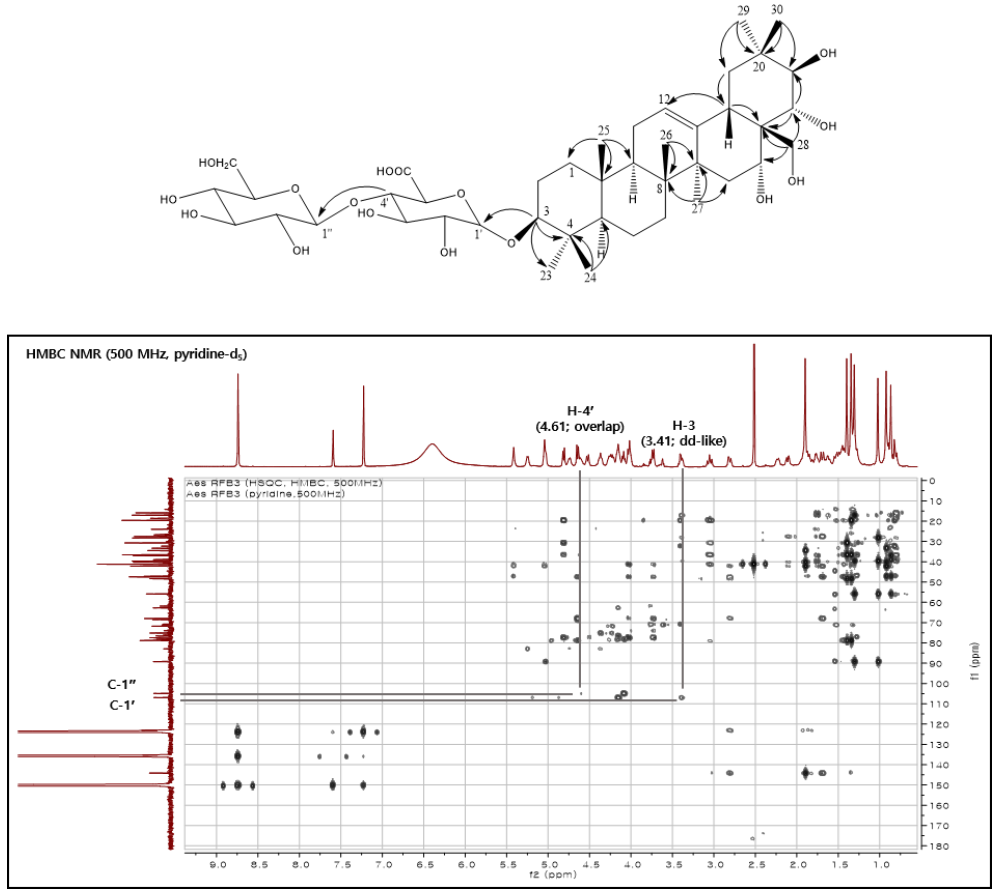


Figure 6. HMBC spectrum of compound **3**

1-4. Compound **4**

Compound **4** was obtained as white amorphous powder with $[\alpha]_{20}^{D}$ + 21.7 (*c*, 0.2, pyridine). IR spectrum presented hydroxyl (3430 cm^{-1}). ^{1}H and ^{13}C NMR data of **4** proposed the structure as an olean-12-ene triterpenoid, showing the presence of six tertiary methyl groups at 1.87 (CH_3-27), 1.56 (CH_3-23), 1.42 (CH_3-30), 1.36 (CH_3-29), 0.94 (CH_3-25), 0.93 (CH_3-26), as well as an olefinic proton at 5.44 (br s, H-12) with two olefinic carbons at 144.4 (C-13) and 123.4 (C-12).

Based on above deductions and comparing spectrum to reference (Chen, Takeda & Ogihara, 1985), compound **4** was determined as protoescigenin.

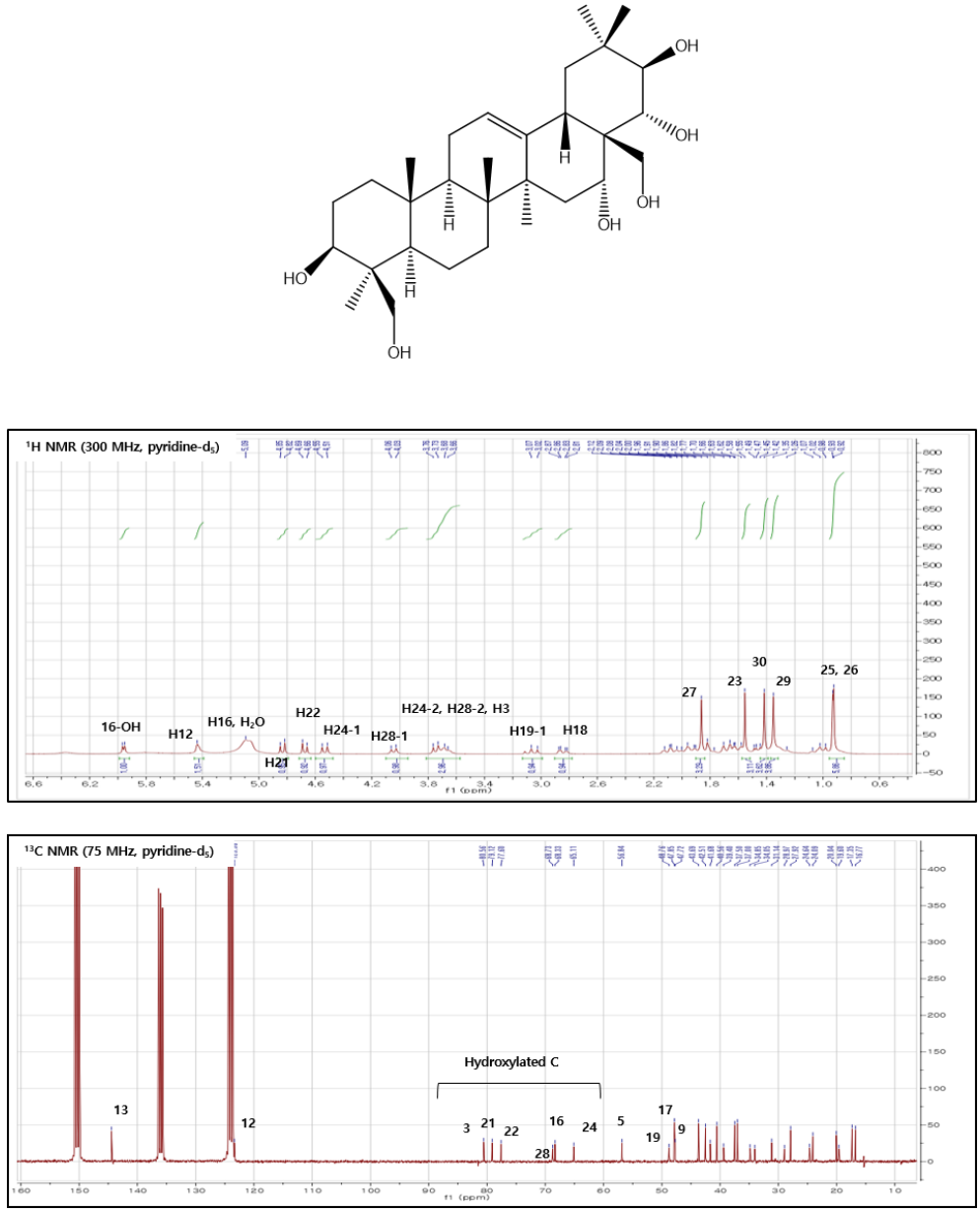
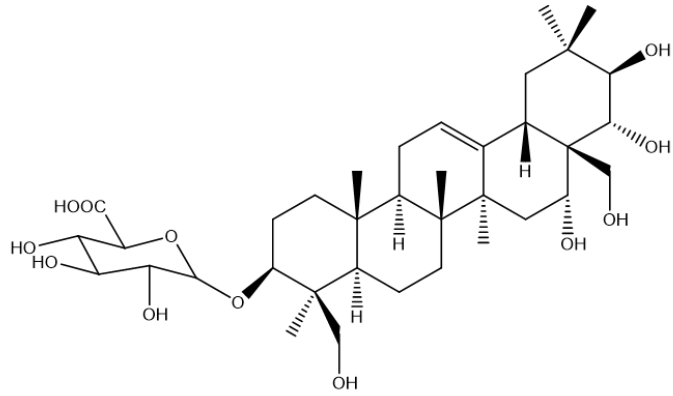
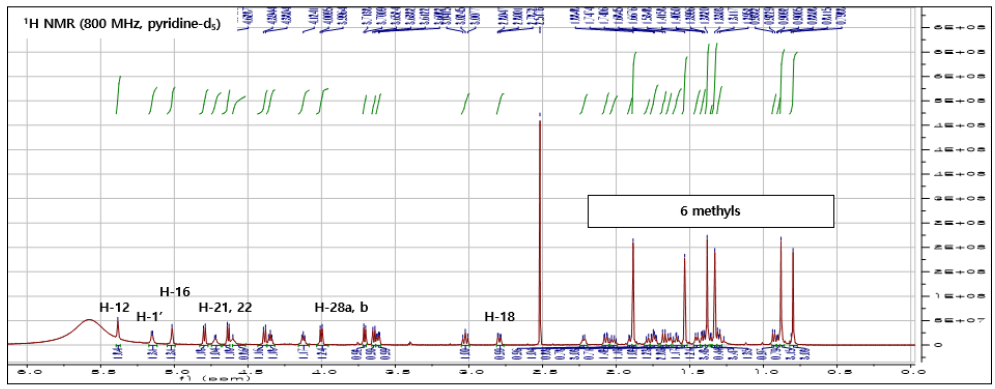


Figure 7. ^{1}H, ^{13}C NMR spectra of compound **4**

1-5. Compound **5**

Compound **5** was obtained as a brown amorphous powder. HRESIMS of positive mode showed a $[(M+H)+[-H_2O]]^+$ ion at *m/z* 665.3898 (calcd for 665.3895) and $[M-H]^-$ ion at *m/z* 681.3852 (calcd for 681.3856), which indicated a molecular formula of $C_{36}H_{58}O_{12}$. Absorption bands at 3385, 1657, 1028 cm^{-1} in the IR spectrum exhibited the presence of hydroxyl, olefinic bond, and glycosidic linkage, respectively. ^1H and ^{13}C NMR data of **5** indicated the structure as an olean-12-ene triterpenoid glucopyranosiduronic acid, disclosing the presence of six tertiary methyl groups [δ_H 0.80 (CH_3-25), 0.88 (CH_3-26), 1.33 (CH_3-29), 1.40 (CH_3-30), 1.53 (CH_3-23), 1.88 (CH_3-27)], as well as an olefinic proton at δ_H 5.38 (br s, H-12) with two olefinic carbon signals at δ_C 123.2 (C-12) and 144.2 (C-13), and one *β*-D-glucopyranosiduronic acid moiety [one anomeric proton δ_H 5.18 (d, J = 7.2 Hz, H-1′), along with six carbon signals at δ_C 173.4 (C-6′), 106.7 (C-1′), 78.4 (C-3′), 78.3 (C-5′), 75.7 (C-2′), and 73.9 (C-4′)]. Compound **5** showed similar with **2** except for the presence of hydroxyl group at C-24 (δ_C 63.6) in **5** compared to those of the ^1H and ^{13}C NMR data of **2**. The HMBC correlation between H-3 (δ_H 3.63) and C-1′ (δ_H 106.7) confirmed the position of *β*-D-glucopyranosiduronic acid. Relative configuration of **5** was investigated by analysis of ROESY spectrum. Correlations between H_2-24 (4.40)/H_3-25 (0.80), H_3-25 (0.80)/H_3-26 (0.88), H_3-26 (0.88)/H_2-28 (4.00), H_2-28 (δ_H 4.00)/H-16 (δ_H 5.02), H-16 (δ_H 5.02)/H-22 (δ_H 4.64), H-22 (δ_H 4.64)/H_3-30 (δ_H 1.40), H_3-30 (δ_H 1.40)/H-18 (δ_H 2.80), and H-18 (δ_H 2.80)/H-22 (δ_H 4.64) were observed in the ROESY data, implying all these protons were on the same side of the molecule. Relative configuration of compound **5** remained unaltered even after two-step reaction except for the deacylation and the cleavage of glucose linkage. Therefore, the structure of **5** was identified as (3*β*,16*α*,21*β*,22*α*)-16,21,22,24,28-pentahydroxyolean-12-en-3-O-*β*-D-glucopyranosiduronic acid.





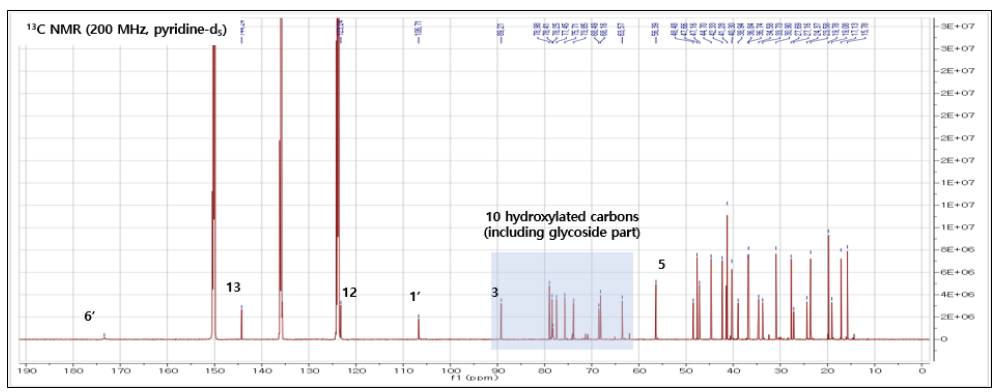
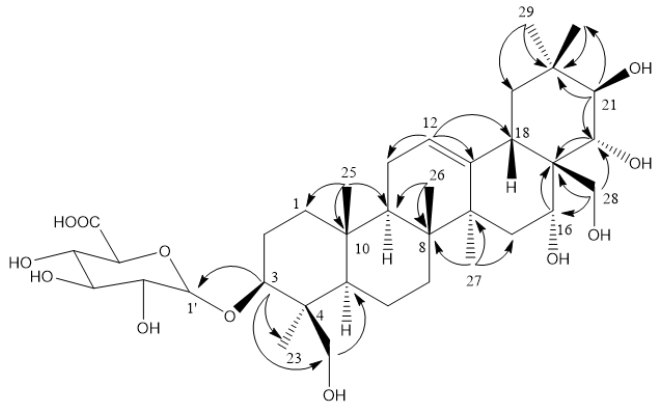


Figure 8. ^{1}H, ^{13}C NMR spectra of compound **5**



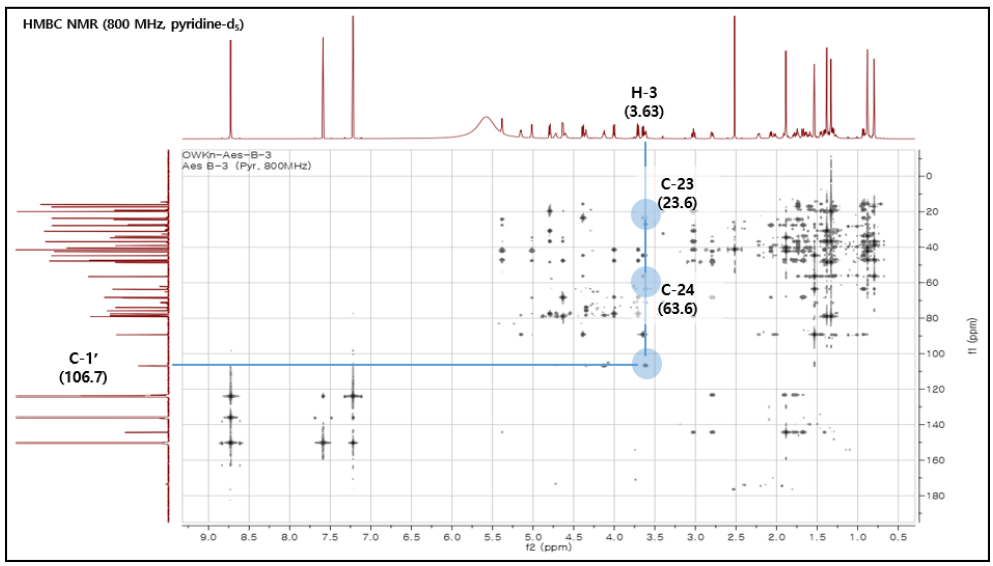
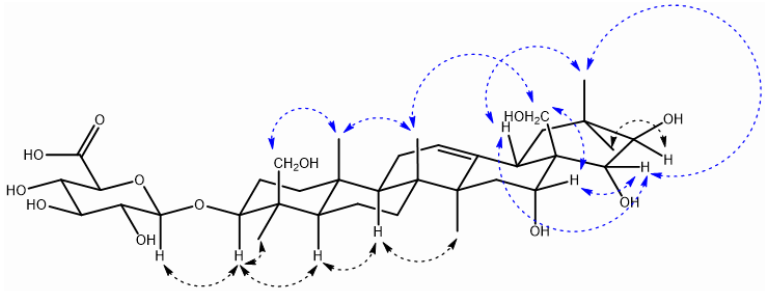


Figure 9. HMBC spectrum of compound **5**



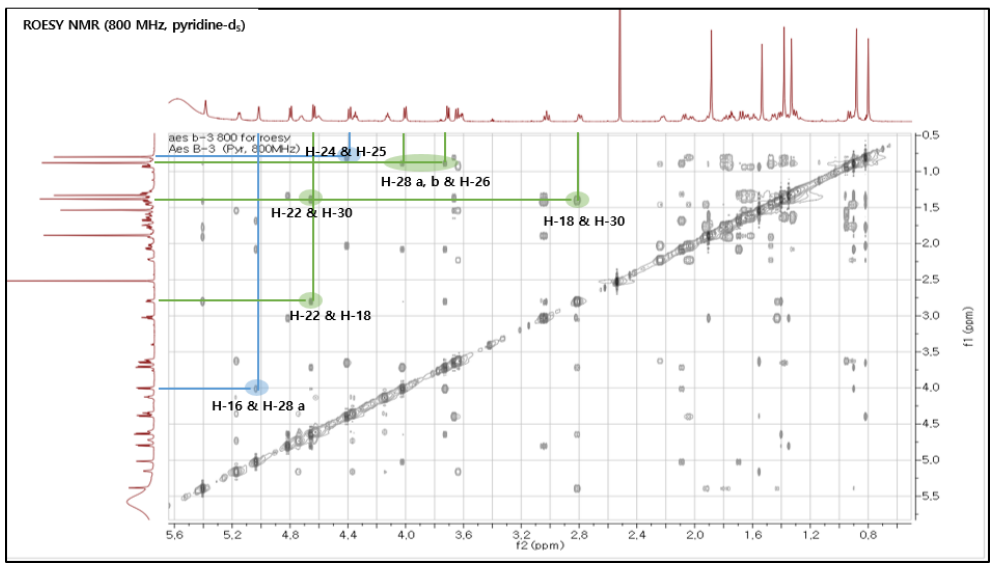
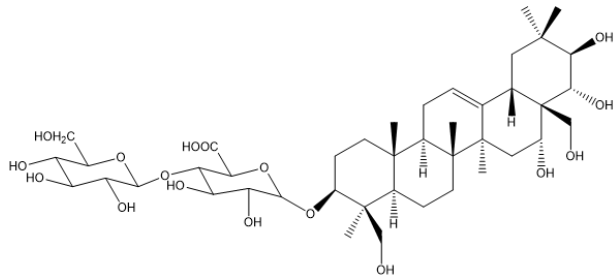
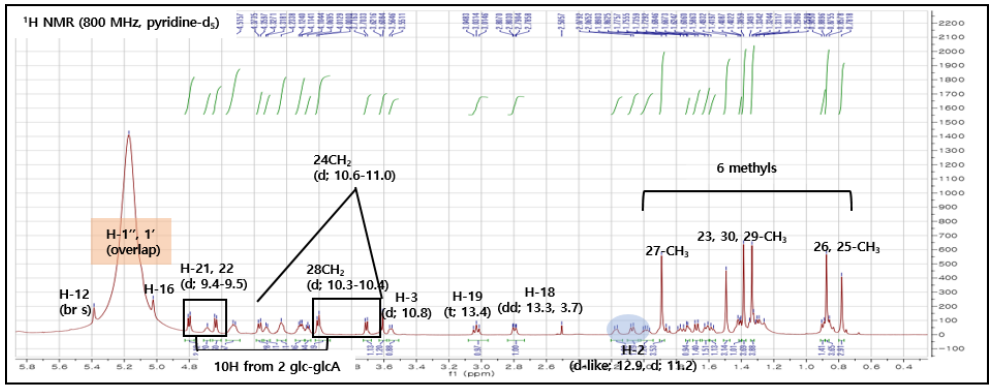


Figure 10. ROESY spectrum of compound **5**

1-6. Compound **6**

Compound **6** was isolated as a brown amorphous powder, with the molecular formula $C_{42}H_{68}O_{17}$, by the HRESIMS at *m/z* 867.4345 $[M+Na]^+$ (calcd for $C_{42}H_{68}O_{17}Na^+$, 867.4349) and at *m/z* 843.4384 $[M-H]^-$ (calcd for $C_{42}H_{67}O_{17}^-$, 843.4384). Its IR spectrum displayed strong absorptions for hydroxyl (3405 cm^{-1}), olefinic bond (1604 cm^{-1}), and glycosidic linkage (1033 cm^{-1}). ^1H and ^{13}C NMR data of **6** suggested the structure as an olean-12-ene triterpenoid glycopyranosyl glucopyranosiduronic acid, exhibiting signals for six tertiary methyl groups [δ_H 0.78 (CH_3-25), 0.88 (CH_3-26), 1.33 (CH_3-29), 1.39 (CH_3-30), 1.49 (CH_3-23), 1.89 (CH_3-27)], an olefinic proton at δ_H 5.39 (br s) with two olefinic carbon signals at δ_C 123.3 (C-12) and 144.3 (C-13), one *β*-D-glucopyranosiduronic acid moiety [an anomeric proton at δ_H 5.09 (H-1′), along with five carbon signals at δ_C 106.2 (C-1′), 83.9 (C-4′), 76.9 (C-3′), 76.9 (C-5′′), and 75.2 (C-2′)], and one *β*-D-glycopyranosyl moiety [one anomeric proton at δ_H 5.22 (H-1′′), along with six carbon signals at δ_C 105.3 (C-1′′), 78.8 (C-5′′), 78.4 (C-3′′), 75.4 (C-2′′) and 72.0 (C-4′′), 62.9 (C-6′′)]. ^{13}C NMR spectra for compound **6** were very close to those for **3**. In particular, the signals for carbons of the glycopyranosyl and glucopyranosiduronic acid moiety of **6** were fully in agreement with those of **3**, indicating the presence of *β*-D-glycopyranosyl-(1→4)]-*β*-D-glucopyranosiduronic acid. Linkage position was further confirmed in the HMBC experiment, showing the correlation from H-1′ (δ_H 5.09) of the *β*-D-glucopyranosiduronic acid to C-3 (δ_C 89.3) and from H-1′′ (δ_H 5.22) of the *β*-D-glycopyranosyl to C-4′ (δ_C 83.9) of the *β*-D-glucopyranosiduronic acid. Thus, compound **6** was concluded as (3*β*,16*α*,21*β*,22*α*)-16,21,22,24,28-pentahydroxyolean-12-en-3-yl-O-[*β*-D-glycopyranosyl-(1→4)]-*β*-D-glucopyranosiduronic acid.





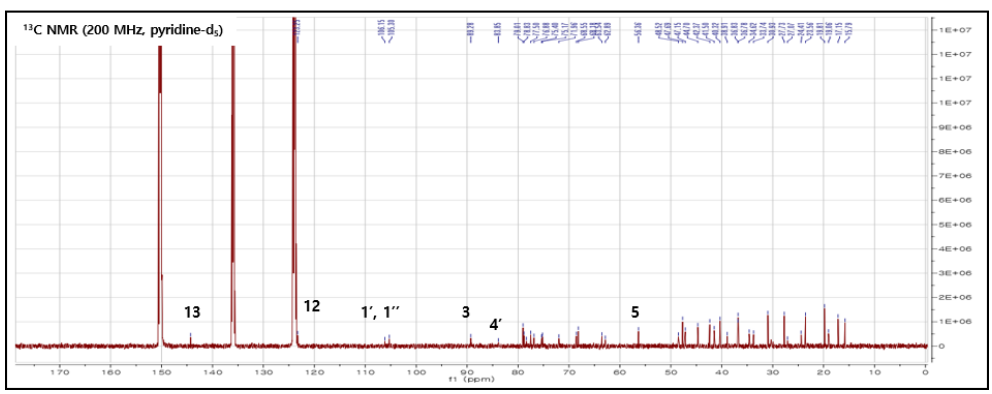
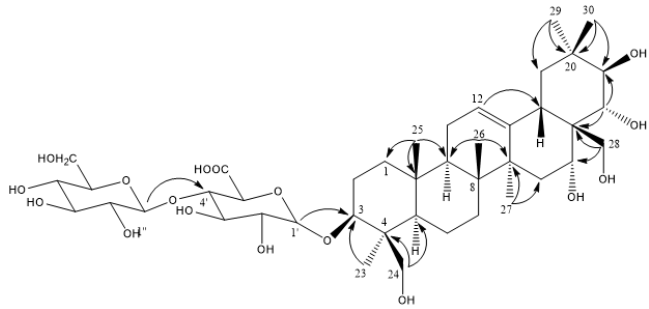


Figure 11. ^{1}H, ^{13}C NMR spectra of compound **6**



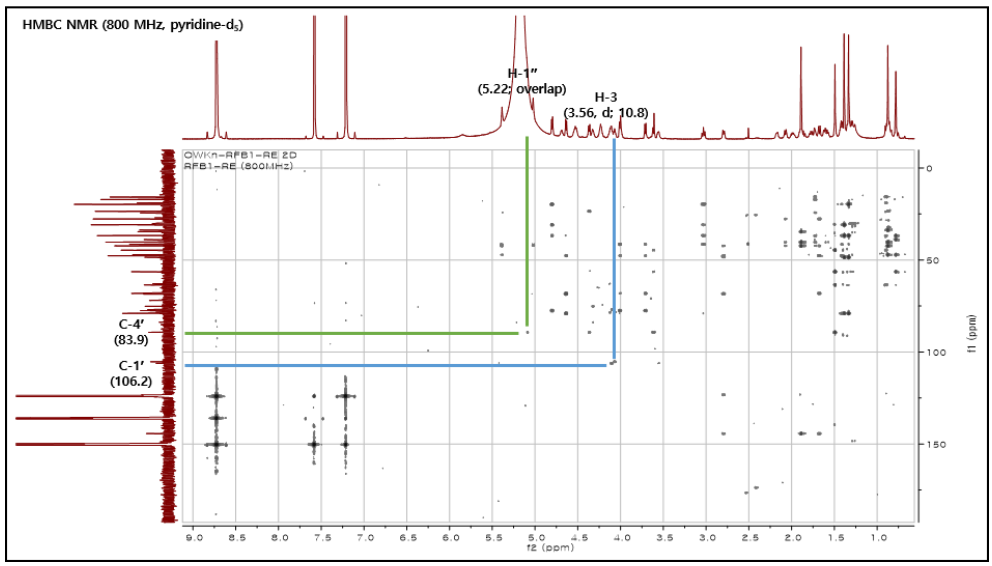
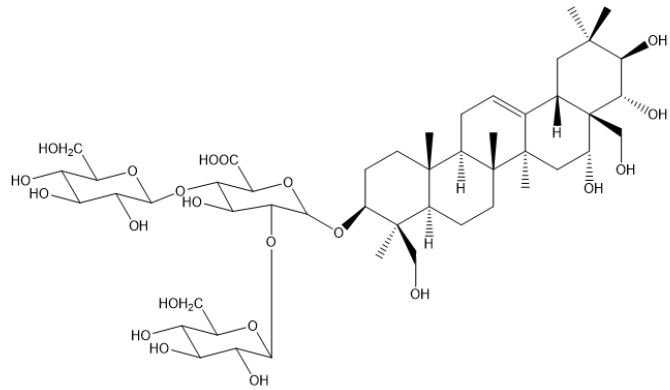
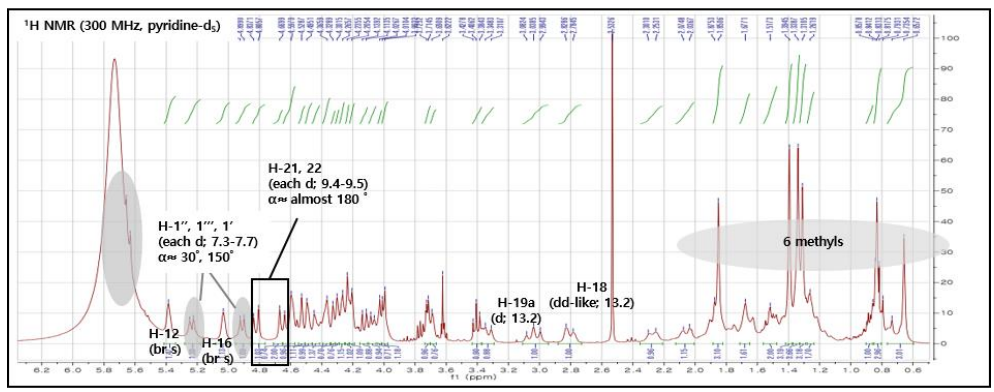


Figure 12. HMBC spectrum of compound **6**

1-7. Compound **7**

^{1}H and ^{13}C NMR spectra of compound **7** showed signals three anomeric protons [5.66 (H-1′′, d; 7.8), 5.25 (H-1′′′, d; 7.3), 4.93 (H-1′, d; 7.4)] and three anomeric carbons [104.9 (C-1′), 104.5 (C-1′′ and C-1′′′)]. An olefinic proton at δ_H 5.38 (br s) with two olefinic carbon signals at δ_C 123.1 (C-12) and 144.2 (C-13) were also presented, indicating the aglycone of **7** was protoescigenin (**4**) moiety. Based on above spectral observation and comparison to the data of reference, compound **7** was structurally deduced as aescuuluside B (Yoshikawa, et al., 1996).





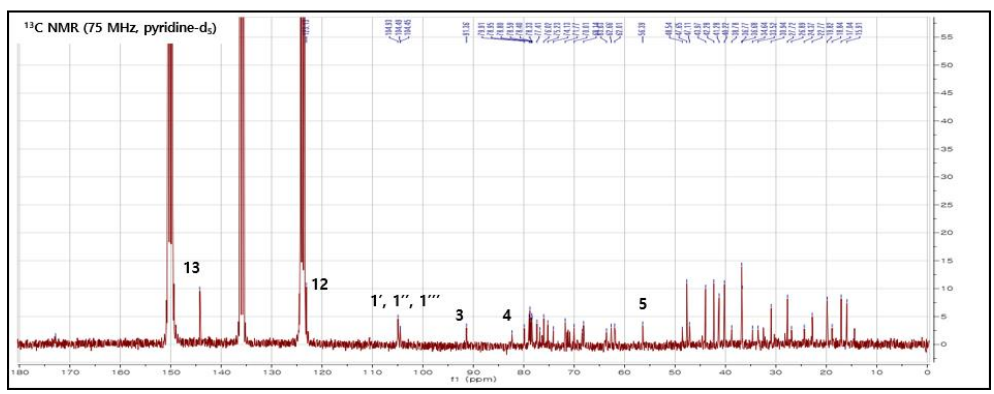
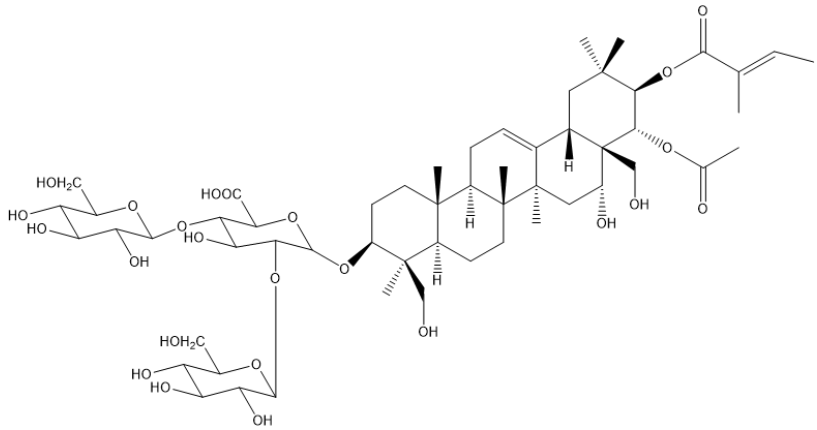


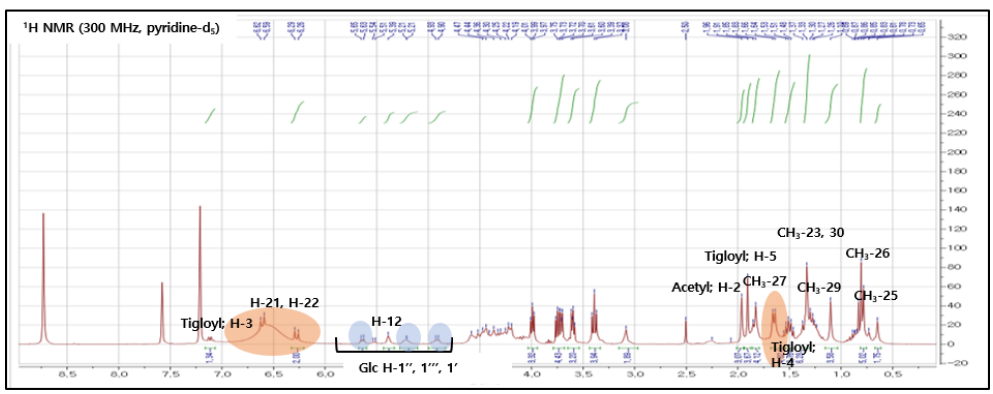
Figure 13. ^{1}H, ^{13}C NMR spectra of compound **7**

1-8. Compound **8**

^{1}H and ^{13}C NMR spectra of compound **8** indicated signals assignable to a tigloyl group [δ_H 7.12 (H‴′-3, d; 7.1), 1.89 (5‴′-CH_3, s), 1.65 (4‴′-CH_3, d; 7.0)] and an acetyl group [δ_H 1.95 (2‴′′-CH_3, s)], along with two methine protons on carbons bearing an acyl group [δ_H 6.61 (H-21, d; 9.9), 6.28 (H-22, d; 10.1)]. Three sugars were also observed by the presence of three anomeric protons at 5.65 (H-1′′, d; 7.5), 5.21 (H-1‴, d-like), 4.92 (H-1′, d; 6.8).

1D NMR data were consistent to those of known compound escin Ia (Yoshikawa, et al., 1996). This was further supported by the co-apperance of protonated and deprotonated peaks in ESI-MS spectrum (*m/z* 1153.4 $[M+Na]^+$, 1129.3 $[M-H]^-$)





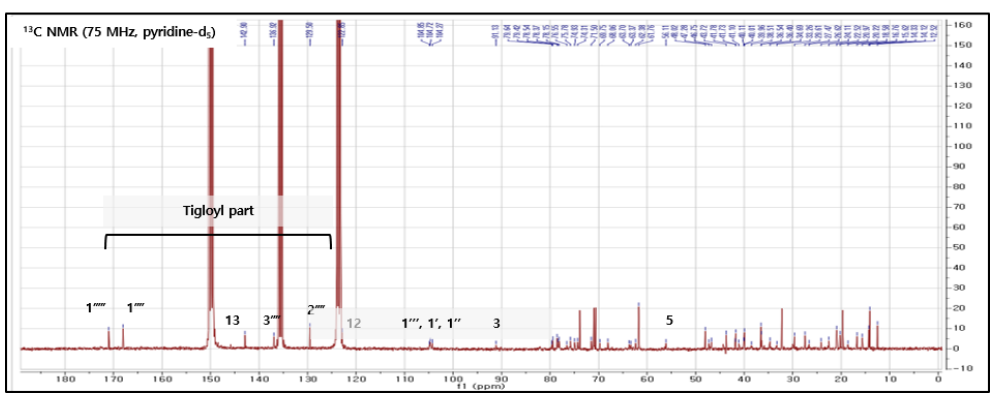
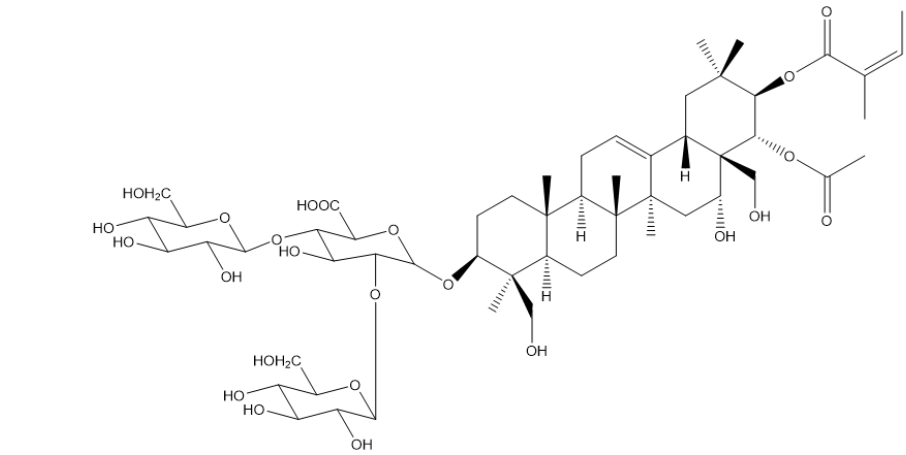
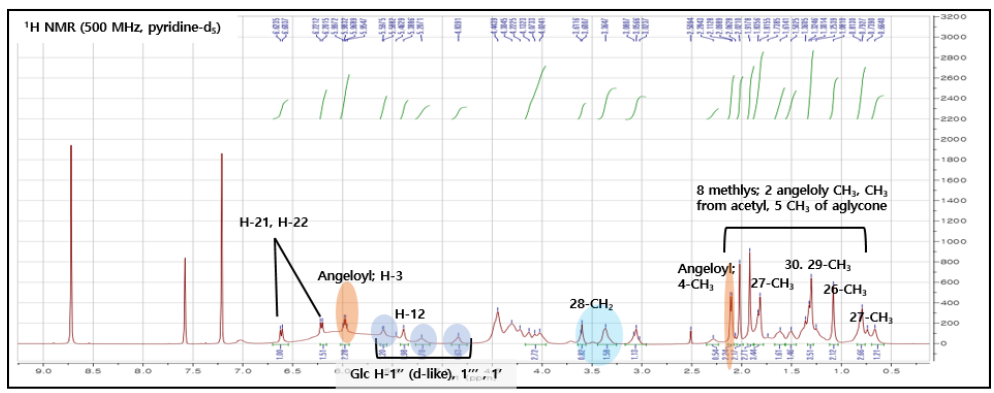


Figure 14. ^{1}H, ^{13}C NMR spectra of compound **8**

1-9. Compound **9**

Compound **9** was isolated as brown amorphous powder with *m/z* 1153.5 $[M+Na]^+$, 1129.3 $[M-H]^-$, which was same as that of compound **8**. The NMR data showed the characteristic angeloyl group [δ_H 5.98 (Ang-H‴-3, dq; 7.2), 2.11 (Ang-4‴-CH_3, d; 7.0), 1.92 (Ang-5‴-CH_3, s)] and an acetyl group [δ_H 2.02 (2⁗-CH_3, s)], together with two methine protons on carbons bearing an acyl group [δ_H 6.62 (H-21, d; 9.9), 6.22 (H-22, d; 9.9)]. Except for linkage of an angeloyl group at C-21, all NMR spectra were consistent with compound **8**, deducing the structure of **9** as escin Ib (Yoshikawa, et al., 1996).





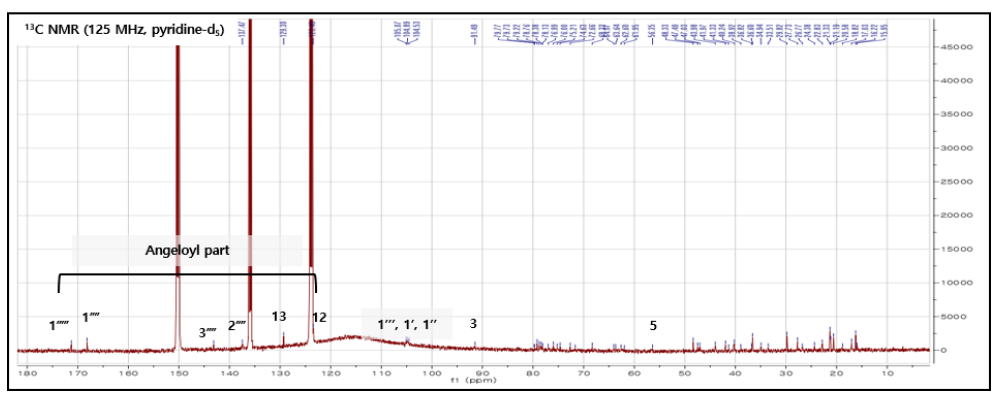
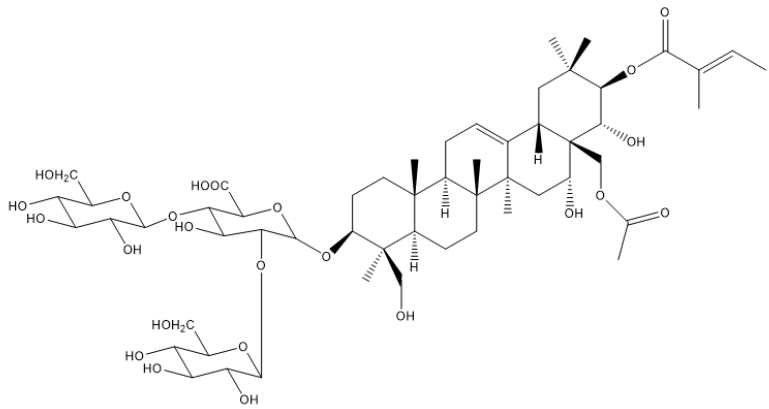


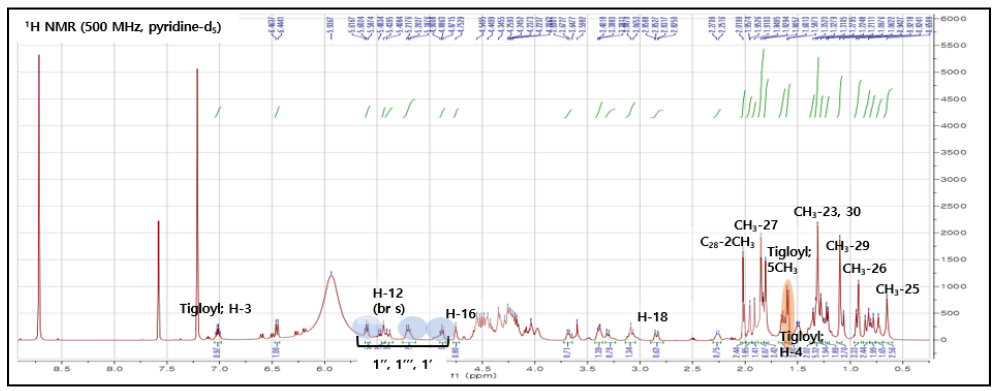
Figure 15. ^{1}H, ^{13}C NMR spectra of compound **9**

1-10. Compound **10**

^{1}H and ^{13}C NMR spectra of compound **10** showed signals due to two acyl groups, a tigloyl group [δ_H 7.02 (H-1‴′, d; 6.4), 1.85 (5‴′-CH_3, s), 1.60 (2‴′-CH_3, d; 7.1)] and an acetyl group [δ_H 2.02 (2‴′′-CH_3, s)]. Three sugars were also detected by the presence of three anomeric protons at 5.60 (H-1′′, d; 7.2), 5.22 (H-1‴, d; 7.5), 4.89 (H-1′, d; 7.4) and three anomeric carbons at 105.0 (C-1′, C-1‴), 104.6 (C-1′′).

1D NMR spectrum were consistent to those of known compound Isoescin Ia (Yoshikawa, Murakami, Yamahara & Matsuda, 1998). This was further supported by the co-apperance of protonated and deprotonated peaks in ESI-MS spectrum (*m/z* 1153.4 $[M+Na]^+$, 1129.3 $[M-H]^-$)





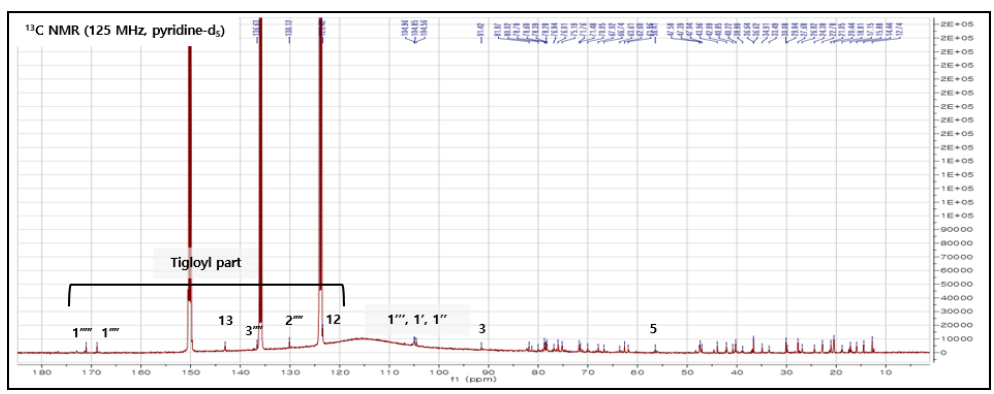
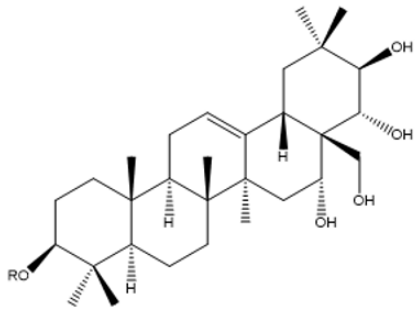
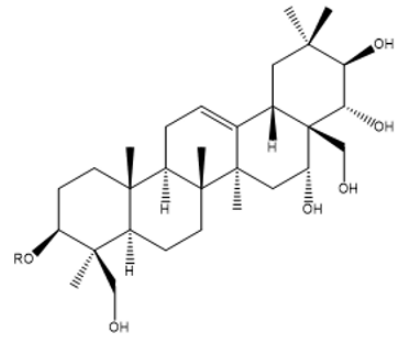


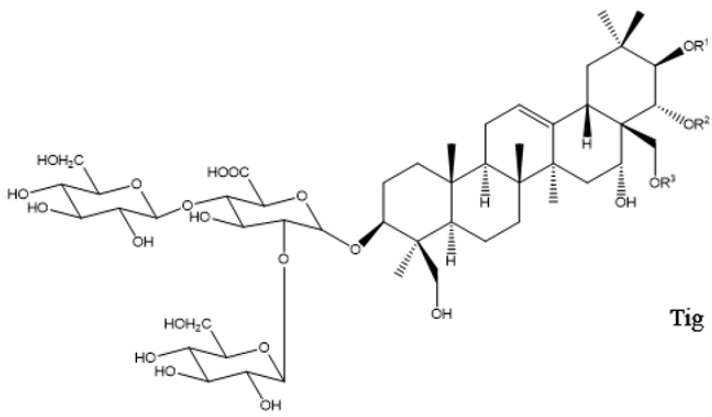
Figure 16. ^{1}H, ^{13}C NMR spectra of compound **10**



	R
1	H
2	glcA
3	glc-glcA (4→1)



	R
4	H
5	glcA
6	glc-glcA (4→1)



	R^1	R^2	R^3
7	H	H	H
8	Tig	Ac	H
9	Tig	H	Ac
10	Ang	Ac	H

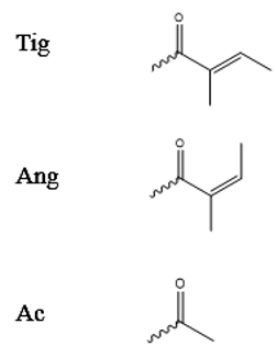


Figure 17. Structures of compounds isolated from the seeds of *Aesculus turbinata*

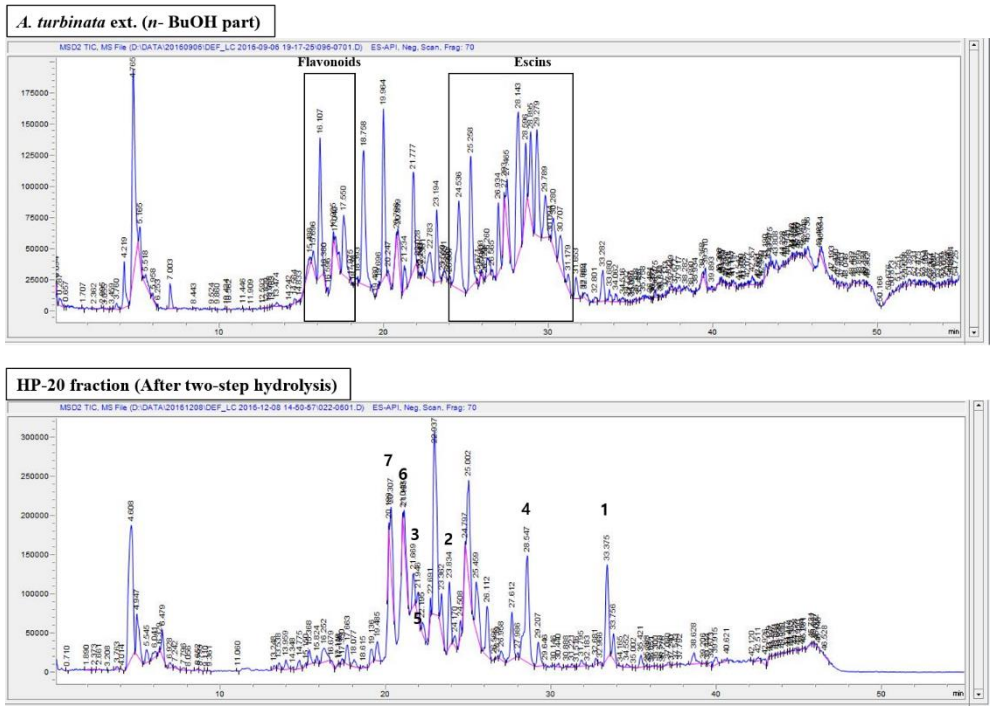


Figure 18. Negative ESI-MS spectrum comparison between n-BuOH part from extract and reaction part from a two-step hydrolysis

2. Cytotoxicity of fractions and isolated compounds

The cytotoxicity assay was done at concentration of 10 μg/mL to compare the cytotoxic effects of the total extract and partitioned fractions before and after a two-step hydrolysis (Fig. 19). The *n*-BuOH fraction, containing a large amount of escins, showed strong cytotoxicity compared to fractions obtained after the two-step hydrolysis. Interestingly, compounds **1**-**7** isolated from the fraction with the two-step hydrolysis were evaluated to have much lower cytotoxic effects than compounds **8**-**10** from the *n*-BuOH part at concentration of 20 μM (Fig. 20). Additionally, dose-dependent cytotoxic effects of compounds **8**-**10** were ascertained at concentrations of 2, 5 and 10 μM (Fig. 21).

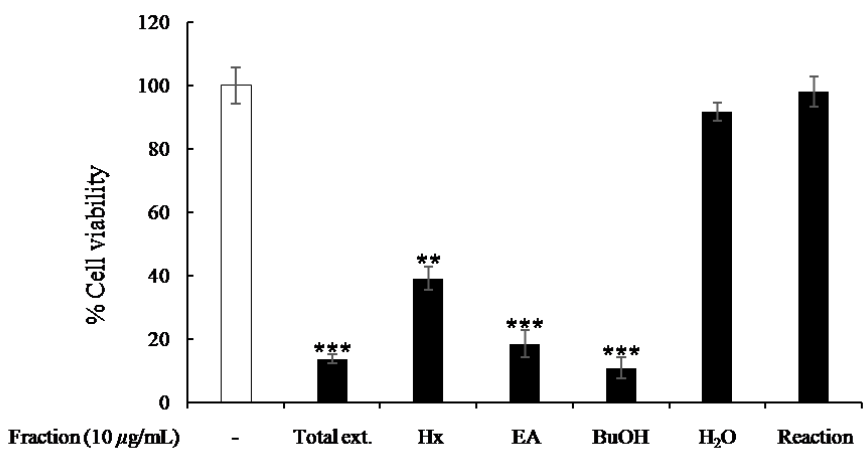


Figure 19. Cytotoxicity assay of fractions in 10 μg/mL

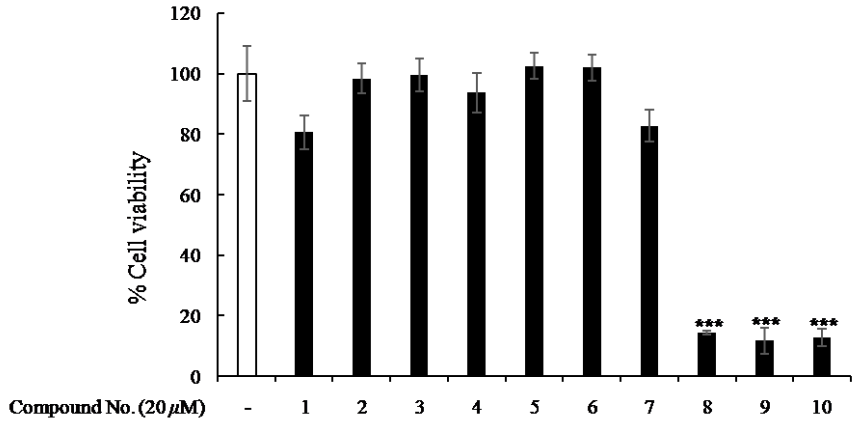


Figure 20. Cytotoxicity assay of compounds **1**-**10** at a concentration of 20 μM

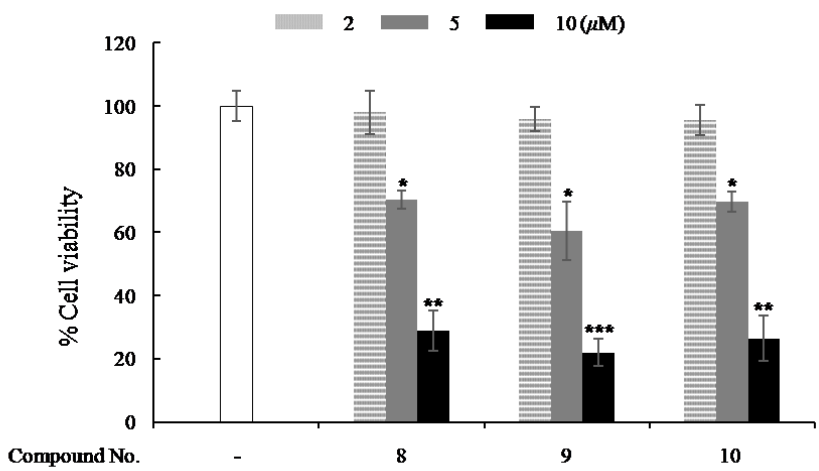


Figure 21. Cytotoxicity assay of compounds **8**, **9** and **10** at concentrations of 2, 5 and 10 μM.

3. PEDV inhibitory activities of fractions and isolated compounds

3-1. Evaluation of PEDV inhibitory activities by CPE assay

The *n*-BuOH fraction and a fraction from a two-step hydrolysis were evaluated for their PEDV inhibitory activities with azauridin as positive control at 1, 2, 5, and 10 μg/mL (Fig. 22). Up to 2 μg/mL, both fractions showed similar, mild inhibitory effects on PEDV replication, proving the original horse chestnut's antiviral activities. Fraction after a two-step hydrolysis inhibited PEDV replication in a dose-dependent manner without cytotoxicity. The *n*-BuOH fractions above 5 μg/mL, which are expected to contaiin many much escins, exhibited poor cell viability because of strong cytotoxic effects, even if it could show better PEDV inhibitory effects than fraction from a two-step hydrolysis. Based on these data, the ten purified oleanane triterpenoids (**1**-**10**) were evaluated for their PEDV inhibitory effects with the same methods (Fig. 23). As compounds **8**-**10** showed strong cytotoxic effects on Vero cells at 20 μM, their PEDV inhibitory activities were evaluated at a concentration of 2 μM. Compounds **1**-**7** were tested at a concentration of 20 μM to compare their inhibitory effects on PEDV replication, providing less cytotoxicity in relatively high concentrations. Compound **4** showed the strongest inhibitory activity among ten compounds **1**-**10**. Additionally, Figure 24 revealed that compounds **4**-**6** exhibited concentration-dependent inhibition of PEDV replication at concentrations of 10, 20 and 40 μM, indicating improved cell viability from the two-step hydrolysis..

Based on cytotoxicity and CPE assays, structure-activity relationships (SARs) were studied. Isolated compounds **1**-**10** from escins and their derivatives after the two-step hydrolysis suggested the presences of three important groups: (1) acylation at C-21, C-22 or C-28 (**1**-**7** and **8**-**10**), (2) methylation at C-24 (**1**-**3** and **4**-**6**), (3) existence of glycosidic linkages [(**1**-**3**) and (**4** and **5**-**7**)]. Group 1 (**1**-**7** and **8**-**10**) indicated that deacylation at C-21 could improve the cell viability (Fig. 20 and Fig. 22). The PEDV inhibitory effects of group 2 (**1**-**3** and **4**-**6**) demonstrated that methylation at C-24 could reduce antiviral activity (Fig. 23). Group 3 [(**1**-**3**) and (**4** and **5**-**7**)] showed that the absence of glycosidic linkage also improved the antiviral effects (Fig. 23).

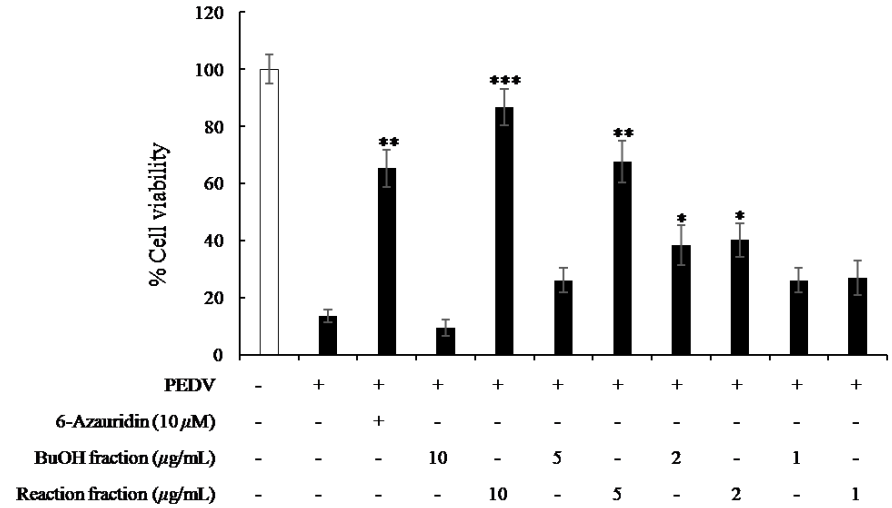


Figure 22. CPE inhibition assay of *n*-BuOH fraction and reaction fraction in 1, 2, 5, and 10 μg/mL.

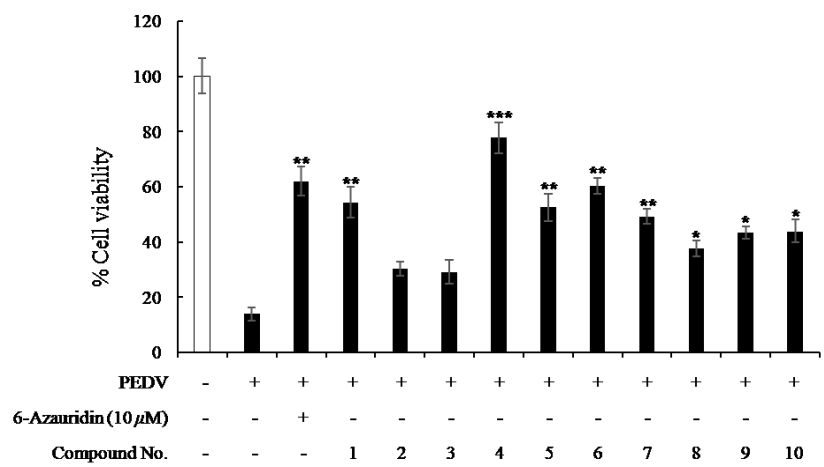


Figure 23. Inhibitory effects of compounds **1**-**10** on PEDV replication in Vero cells

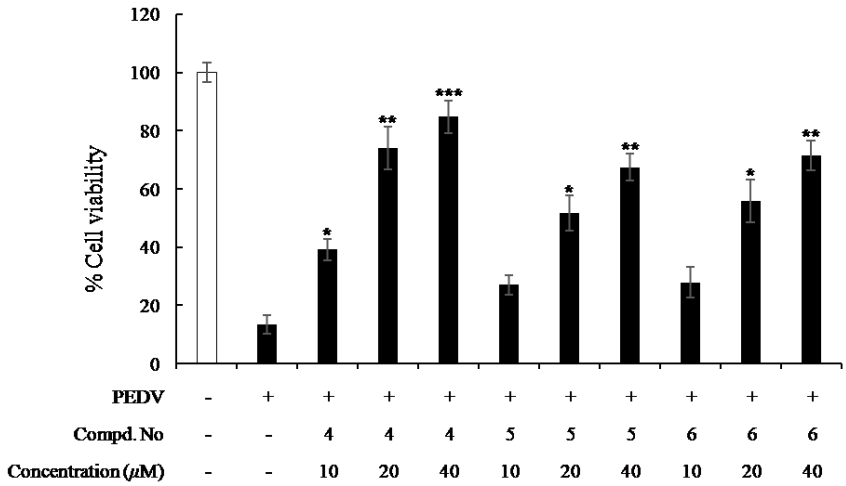


Figure 24. Inhibition of PEDV replication by compounds **4**-**6** at concentrations of 10, 20, and 40 μM

3-2. Evaluation of PEDV inhibitory activities by Western blot assay

During the PEDV replication, two key structural proteins, spike and nucleocapsid proteins, take part in important roles (Song & Park, 2012). The spike protein regulates the entry stage of the virus (Cruz, Kim & Shin, 2008), and binding of nucleocapsid protein to viral RNA is crucial for viral transcription (Baric, et al., 1988). Following the data of the cytotoxicity and CPE assays (Fig. 20-23), five compounds **1** and **4**-**7** were selected for further evaluation. First, the inhibitory effects of compounds **1** and **4**-**7** on nucleocapsid protein synthesis at 20 μM were measured using Western blot (Fig. 25). Five compounds showed moderate inhibitory effects on nucleocapsid protein synthesis, and compound **4** significantly inhibited nucleocapsid protein synthesis. Thus, compound **4** was further analysed for its effects in nucleocapsid and spike protein synthesis with Western blot at concentrations of 10, 20 and 40 μM and it was found to inhibit PEDV replication in concentration-dependant manner (Fig. 26).

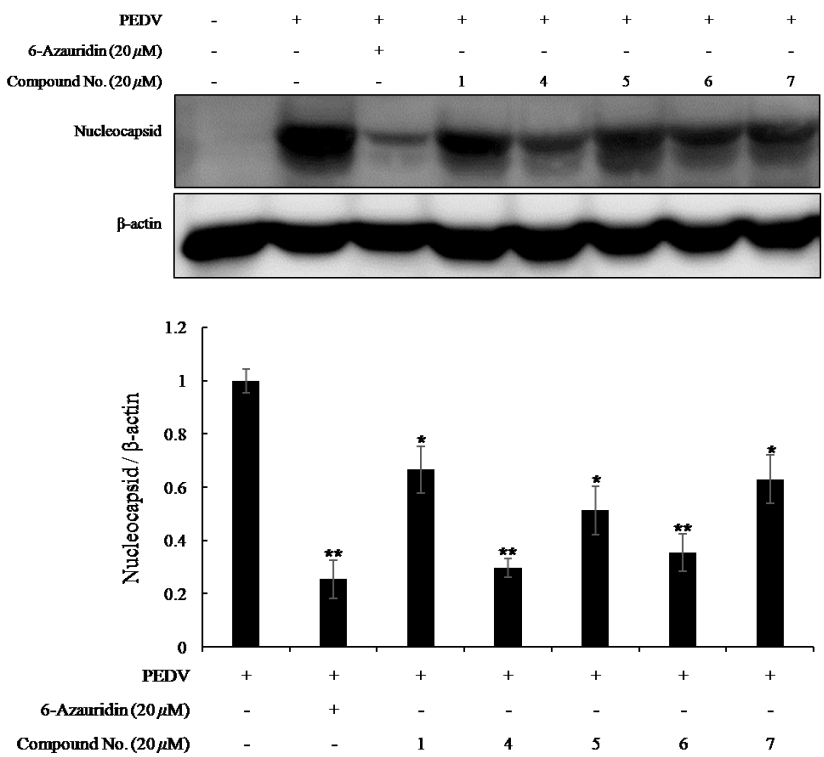


Figure 25. Inhibitory effects of compounds **1**, **4**, **5**, **6**, and **7** on PEDV nucleocapsid synthesis, using Western blot assay

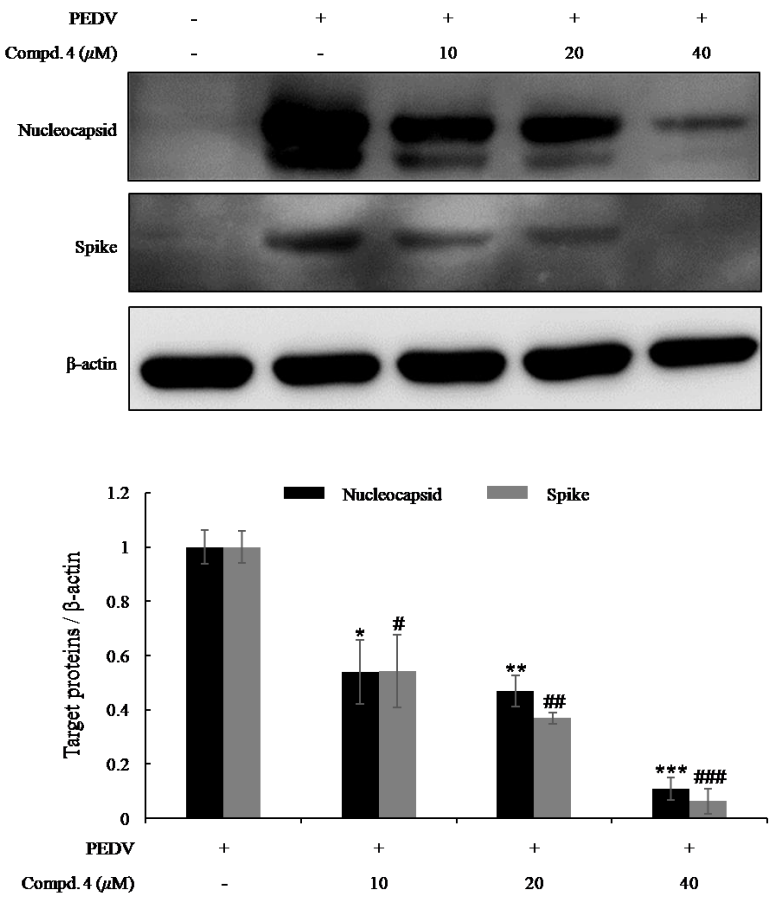


Figure 26. Inhibitory effects of compound **4** on PEDV nucleocapsid and spike protein synthesis, using Western blot analysis

3-3. Evaluation of PEDV inhibitory activities by real-time PCR

On the basis of the above findings, compounds **4** and **6** were also were measured with key genes and proteins crucial for PEDV replication by real time PCT (RT-PCR). To measure the expression level of viral RNA encoding nucleocapsid and spike proteins, compounds **4** and **6** were treated in Vero cells at a concentration of 40 μM and total RNA was extracted for reverse transcription followed by polymerase chain reaction using the primers for PEDV (Table 3). Figure 27 showed the RNA expression levels of two kinds of proteins with compounds **4**, **6** and positive control. When the inhibitory effects of compound **4** were analysed in detail at the concentrations of 10, 20 and 40 μM, compound **4** inhibited the RNA expression of nucleocapsid and spike proteins in dose-dependent manner (Fig. 28).

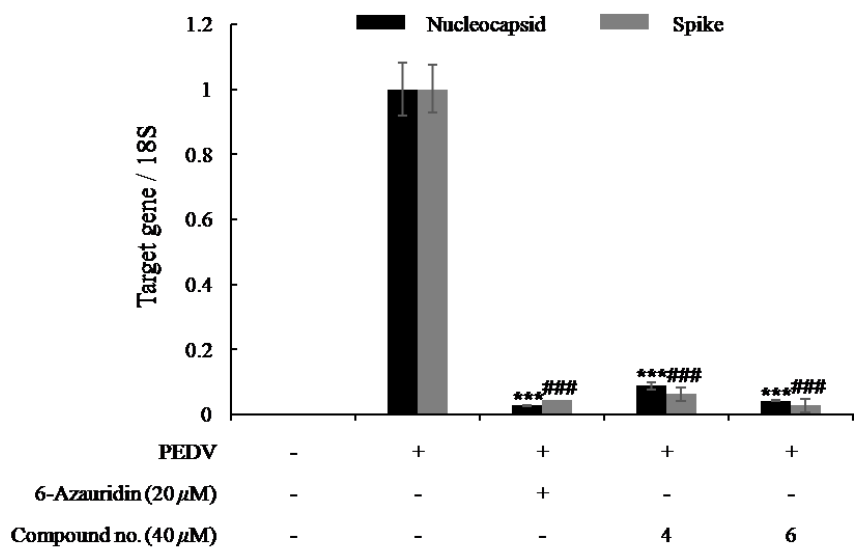


Figure 27. Inhibitory activites of compounds **4** and **6** on PEDV RNA expression encoding nucleocapsid and spike protein estimated by RT-PCR at the concentration of 40 μM.

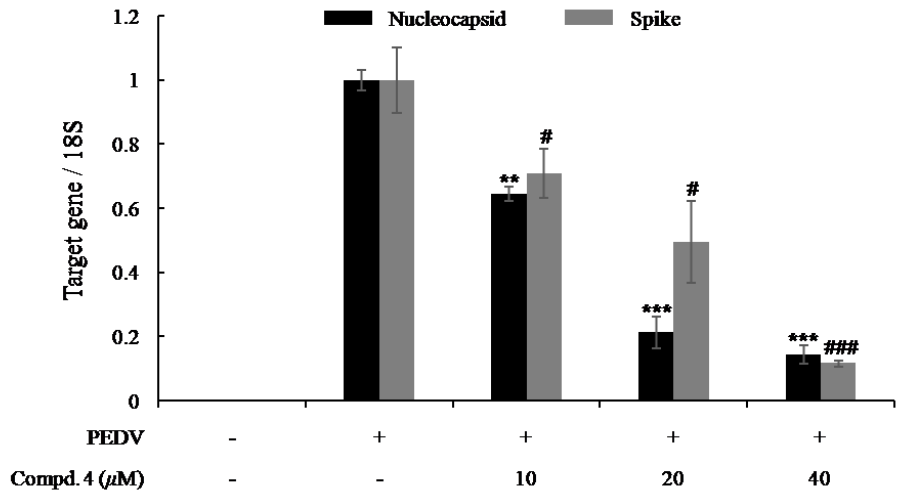


Figure 28. By RT-PCR analysis, compound **4** was analysed for its inhibitory on PEDV RNA expression encoding nucleocapsid and spike protein at the concentration of 10, 20 and 40 μM.

Table 3. Primers used for Real-time PCR.

Primer	**Sequence (5′-3′)**
GP2 spike – forward	GCT AGT GGC GTT CAT GGT ATT TT
GP2 spike – reverse	ACG GCT CTT GCG AAA TGC
GP6 Nucleocapsid – forward	GAA AAT CCT GAC AGG CAT AAG CA
GP6 Nucleocapsid – reverse	TTG CCG CTG TTG TCA GAC TT
18 S – forward	GCT TAA TTT GAC TCA ACA CGG GA
18 S – reverse	AGC TAT CAA TCT GTC AAT CCT GTC

3-4. Evaluation of PEDV inhibitory activities by immunocytochemistry assay

On the basis of features of inhibition of PEDV RNA expression, compound **4** was further studied for its inhibitory effects on PEDV replication, by performing an immunocytochemistry assay (Fig. 29). We observed the green fluorescence in virus-infected cells but no signals in mock-treated cells. This result revealed that compound **4** had noticeable inhibitory effects on PEDV replication in a dose-dependent manner at concentrations of 10, 20 and 40 μM.

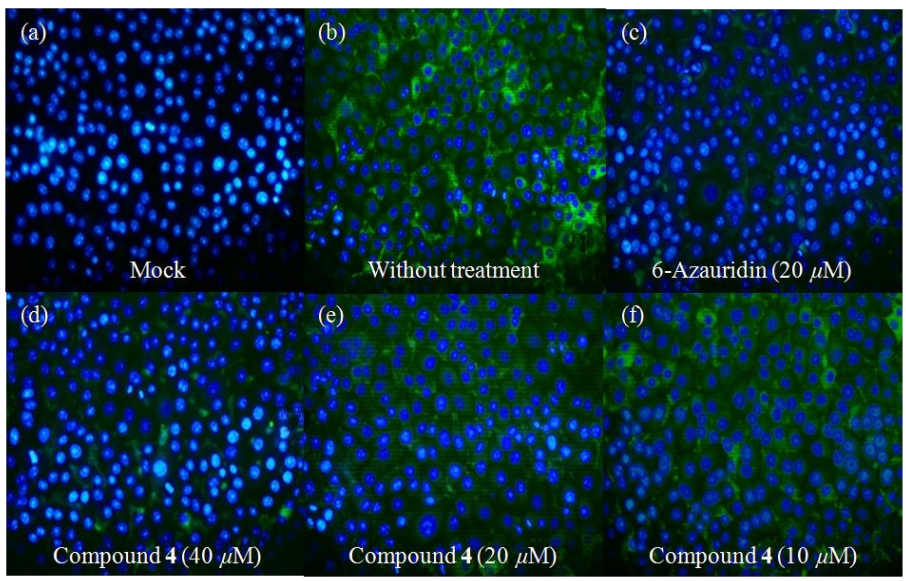


Figure 29. Immunocytochemistry assay showed that PEDV replication was inhibited by compound **4** in dose-dependent manner.

3-5. Computer modelling of SARS-CoV 3CL protease inhibition

3C-Chymotrypsin-Like protease (3CL protease) is vital for proteolytic processing viral replication in coronavirus. As escin was reported as a SARS-CoV 3CL protease inhibitor (C. Wu, et al., 2004), we performed docking modelling of compound **4** into the active site of SARS-CoV $3CL^{pro}$ (PDB ID code 3V3M) (Jacobs, et al., 2013). The binding site was predicted by the 2D program of DS 4.0. As shown in Figure 30, the hydroxyl group of C22 and C16 of **4** formed hydrogen bonds with the oxygen atom of the carbonyl group of Glu166. Additionally, the methyl group of C23 and the B ring of **4** showed hydrophobic interactions with Cys145 and Leu27 through their side chains.

The CDOCKER interaction energy was calculated to be -38.63 kcal/mol. The $3CL^{pro}$ binding energy value of compound **4** was unstable and weaker than that of the reference ligand 0EM. However, clear key amino acid interactions of compound **4** with $3CL^{pro}$, proposed the mode of action as inhibition of 3CL protease and explained that the high concentration of escin derivatives was required to show activities in several experiments.

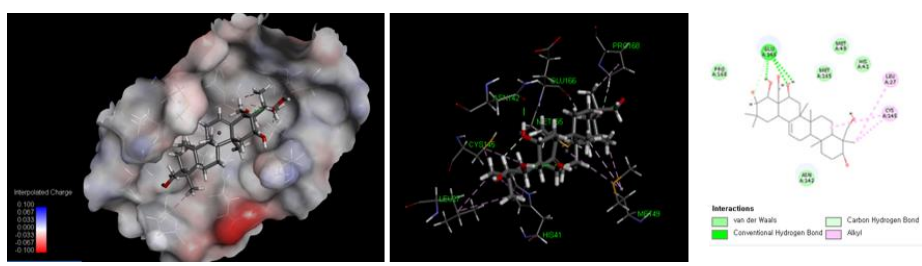


Figure 30. Docking simulation of 3CL protease (PDB: 3V3M) with compound **4** and its interactions.

IV. Conclusions

Including four new compounds (**2**, **3**, **5**, and **6**), ten oleanane-type triterpenoids (**1**-**10**) were isolated from the seeds of *Aesculus turbinata* (Japanese horse chestnut). By a two-step hydrolysis, cytotoxicity of n-BuOH part fraction and their isolated compounds was decreased. Especially two compounds **4** and **6** showed strong inhibitory activities against PEDV in a dose-dependent manner. The present study proposed the way to utilize Japanese horse chestnut for treating PEDV with less cytotoxic effects and also to make for the diversity of bioactive compounds.

V. References

Baric, R. S., Nelson, G., Fleming, J. O., Deans, R. J., Keck, J. G., Casteel, N. & Stohlman, S. A. (1998). Interactions between coronavirus nucleocapsid protein and viral RNAs: implications for viral transcription. *Journal of Virology*, *62(11)*, 4280-4287.

Boheemen, S. V., Graaf, M., Lauber, C., Bestebroer, T. M., Raj, V. S., Zaki, A. M., Osterhaus, A. D. M. E., Haagmans, B. L., Gorbalenya, A. E., Snijder, E. & Fouchier, R. A. M. (2012). Genomic characterization of a newly discovered coronavirus associated with acute respiratory distress syndrome in humans**.** *American Society for Microbiology*, *3(6)*, e00473-12.

Chan, P. K. (2007). Acylation with diangeloyl groups at C21–22 positions in triterpenoid saponins is essential for cytotoxcity towards tumor cells. *Biochemical Pharmacology*, *73(3)*, 341-350.

Chan, P. K., Zhao, M., Che, C. T. & Mak, E. (2008). Cytotoxic acylated triterpene saponins from the husks of *Xanthoceras sorbifolia. Journal of Natural Products*, *71(7)*, 1247-1250.

Chen, Y. J., Takeda, T. & Ogihara, Y. (1985). Studies on the constituents of Xanthoceras sorbifolia BUNGE. III. Minor prosapogenins from the fruits of Xanthoceras sorbifolia BUNGE. *Chemical and Pharmaceutical Bulletin*, *33(1)*, 127-134.

Cruz, D. J. M., Kim, C. & Shin, H. (2008). The GPRLQPY motif located at the carboxy-terminal of the spike protein induces antibodies that neutralize Porcine epidemic diarrhea virus. *Virus Research*, *132(1-2)*, 192-196.

Graham, R. L., Donaldson, E. F. & Baric, R. S. (2013). A decade after SARS: strategies for controlling emerging coronaviruses. *Nature Review Microbiology*, *11(12)*, 836-848.

Hu, J. N., Zhu, X. M., Han, L. K., Saito, M., Sun, Y. S., Yoshikawa, M., Kimura, Y. & Zheng, Y. N. (2008). Anti-obesity effects of escins extracted from the seeds of *Aesculus turbinata* BLUME (Hippocastanaceae). *Chemical and Pharmaceutical Bulletin*, *56(1)*, 12-16.

Jacobs, J., Grum-Tokars, V., Zhou, Ya., Turlington, M., Saldanha, S. A., Chase, P., Eggler, A., Dawson, E. S., Baez-Santos, Y. M., Tomar, Sakshi., Mielech, A. M., Baker, S. C., Lindsley, C. W., Hodder, P., Mesecar, A. & Stauffer, S. R. (2013). Discovery, synthesis, and structure-based optimization of a series of N-(*tert*-Butyl)-2-(*N*-arylamido)-2-(pyridin-3-yl) acetamides (ML 188) as potent noncovalent small molecule inhibitors of the severe acute respiratory syndrome coronavirus (SARS-CoV) 3CL protease. *Journal of Medicinal Chemistry*, *56(2)*, 534-546.

Konoshima, T. & Lee, K. (1986). Antitumor agents, 82. Cytotoxic sapogenols from Aesculus hippocastanum. *Journal of Natural Products*, *49(4)*, 650-656.

Li, C., Li, Z., Zou, Y., Wicht, O., Kuppeveld, F. J. M., Rottier, P. J. M. & Bosch, B. J. (2013). Manipulation of the porcine epidemic diarrhea virus genome using targeted RNA recombination. *PLoS One*, *8(8)*, e69997.

Masters, P. S. (2006). The molecular biology of coronaviruses. *Advances in Virus Research*, 66, 193-292.

Mojzisova, G., Mojzis, J., Pilatova, M., Varinska, L., Ivanova, L., Strojny, L. & Richnavsky, J. (2013). Antiproliferative and antiangiogenic properties of horse chestnut extract. *Phytotherapy Research*, *27(2)*, 159-165.

Piao, S., Kang, M., Lee, Y. J., Choi, W. S., Chun, Y., Kwak, C. & Kim, H. H. (2014). Cytotoxic effects of escin on human castration-resistant prostate cancer cells through the induction of apoptosis and G2/M cell cycle arrest. *Urology*, *84(4)*, 982.e1-982.e7.

Podolak, I., Galanty, A. & Sobolewska, D. (2010). Saponins as cytotoxic agents: a

review. *Phytochemistry Reviews*, *9(3)*, 425-474.

Rimmon, A., Vexler, A., Berkovich, L., Earon, G., Ron, I. & Lev-Ari. S. (2013). Escin chemosensitizes human pancreatic cancer cells and inhibits the nuclear factor-kappaB signaling pathway. *Biochemistry Research International* , *2013*, 1-9.

Sato, I., Kofujita, H., Suzuki, T., Kobayashi, H. & Tsuda, S. (2006). Antiinflammatory effect of Japanese horse chestnut (*Aesculus turbinata*) seeds. *The journal of Veterinary Medical Science*, *68(5)*, 487-489.

Song, D. & Park. B. (2012). Porcine epidemic diarrhea virus: a comprehensive review of molecular epidemiology, diagnosis, and vaccines. *Virus genes*, *44(2)*, 167-175.

Sun, H., Fang, W. S., Wang, W. Z. & Hu, C. (2006). Structure-activity relationships of oleanane- and ursane-type triterpenoids. *Botanical Studies*, *47*, 339-368.

Wang, P., Ownby, S., Zhang, Z., Yuan, W. & Li, S. (2010). Cytotoxicity and inhibition of DNA topoisomerase I of polyhydroxylated triterpenoids and triterpenoid glycosides. *Bioorganic Medicinal Chemistry Letters*, *20(9)*, 2790-2796

Wong, G., Liu, W., Liu, Y., Zhou, B., Bi, Y. & Gao, G. F. (2015). MERS, SARS, and Ebola: the role of super-spreaders in infectious disease. *Cell Host & Microbe*, *18(4)*, 398-401.

Wit, E., Doremalen, N. V., Falzarano, D. & Munster, V. J. (2016), SARS and MERS: recent insights into emerging coronaviruses. *Nature Reviews Microbiology*, *14(8)*, 523-534.

Wu, C-Y., Jan, J. T., Ma, S. H., Kuo, C. J., Juan, H. F., Cheng, Y. S., Hsu, H. H., Huang, H. C., Wu, D., Brik, A., Liang, F. S., Liu, R. S., Fang, J. M., Chen, S. T., Liang, P. H. & Wong, C. H. (2004). Small molecules targeting severe acute

respiratory syndrome human coronavirus. *Proceedings of the National Academy of Sciences of the United States of America, 101(27),* 10012-10017.

Yang, X. W., Zhao, J. & Hattori, M. (2008). Three new triterpenoid saponins from the seeds of *Aesculus turbinata*. *Journal of Asian Natural Products Research*, *10(3)*, 243-247.

Yoshikawa, M., Murakami, T., Matsuda, H., Yamahara, J., Murakami, N. & Kitagawa, I. (1996). Bioactive saponins and glycosides. III. horse chestnut. (1) : The structures, inhibitory effects on ethanol absorption, and hypoglycemic activity of escins Ia, Ib, IIa, IIb, and IIIa from the seeds of *Aesculus hippocastanum* L. *Chemical and Pharmaceutical Bulletin*, *44(8)*, 1454-1464.

Yoshikawa, M., Murakami, T., Yamahara, J. & Matsuda, H. (1998). Bioactive saponins and glycosides. XII. Horse chestnut. (2): Structures of escins IIIb, IV, V, and VI and isoescins Ia, Ib, and V, acylated polyhydroxyoleanane triterpene oligoglycosides, rom the seeds of horse chestnut tree (Aesculus hippocastanum L., Hippocastanaceae). *Chemical and Pharmaceutical Bulletin*, *46(11)*, 1764-1769.

Zaki, A. M., Boheemen, S. V., Bestebroer, T. M., Osterhaus, A. D. & Fouchier, R. A. (2012). Isolation of a novel coronavirus from a man with pneumonia in Saudi Arabia. The *New England Journal of Medicine*, *367(19)*, 1814-1820.

국문초록

칠엽수(*Aesculus turbinata* Bl.)는 무환자나무과(Sapindaceae)에 속하는 낙엽성 교목으로 한국, 일본, 중국 등에 널리 분포한다. 칠엽수 열매에는 escin 이라 하는 triterpenoidal saponin이 다량 함유되어있으며 항암, 항염증, 항바이러스 등의 생리활성을 갖고 있는 것으로 보고되고 있다. 그러나 현재까지 escin 관련 화합물의 돼지 유행성 설사 바이러스(Porcine epidemic diarrhea virus; PEDV)에 대한 연구는 진행된 바 없다. 또한, C-21 혹은 C-22 자리가 아실화되어있는 escin은 강한 세포 독성을 나타내기 때문에 현재까지 칠엽수의 다양한 이용가능성은 제한적이었다.

본 연구에서는 알칼리와 산의 화학반응을 통해 escin의 탈아실화와 당 가수분해 반응을 유도하였고, 이를 통한 세포 독성 및 PEDV 저해 활성 차이를 평가하였다. 칠엽수 열매의 70% 에탄올 추출물을 수득한 후, *n*-Hexane, EtOAc, *n*-BuOH 및 H_2O 층으로 분획하였다. Escin이 많이 함유되어 있는 *n*-BuOH 층에서 산, 알칼리 가수분해 반응을 진행한 후 화합물의 구성성분을 분석한 결과, 천연으로부터 새로운 4종의 oleanane-type triterpenoid 화합물(**2**, **3**, **5** 와 **6**)을 포함하여 총 10종의 관련 화합물(**1**-**10**)을 분리하고 구조동정하였다. 10종의 화합물은 각각, escinidin(**1**), (3β, 16α, 21β, 22α)-16, 21, 22, 28-tetrahydroxyolean-12-en-3-O-β-D-glucopyranosiduronic acid(**2**), (3β, 16α, 21β, 22α)-16, 21, 22, 28-tetrahydroxyolean-12-en-3-yl O-[β-D-glycopyranosyl-(1→4)]-β-D-glucopyranosiduronic acid(**3**), protoescigenin(**4**), (3β, 16α, 21β, 22α)-16, 21, 22, 24, 28-pentahydroxyolean-12-en-3-O-β-D-glucopyranosiduronic acid(**5**), (3β, 16α, 21β, 22α)-16, 21, 22, 24, 28-pentahydroxyolean-12-en-3-yl O-[β-D-glycopyranosyl-(1→4)]-β-D-glucopyranosiduronic

acid(**6**), aesculuside B(**7**), escin Ia(**8**), escin Ib(**9**)와 isoescin Ia(**10**)로 결정하였다.

분리된 화합물의 세포 독성과 PEDV에 대한 저해 활성을 확인한 결과, 반응 전과 후의 *n*-BuOH 층에서 PEDV 저해 활성을 관찰하였다. 또한, *n*-BuOH 층에서 분리한 3종의 화합물(**8**-**10**)에 비해 반응 후의 *n*-BuOH 층에서 분리한 7종의 화합물(**1**-**7**)에서 세포 독성 감소효과를 관찰하였으며, 특히 2종의 화합물(**4**와 **6**)은 농도 의존적으로 PEDV 저해 활성이 있음을 확인하였다.

본 연구의 결과는 escin의 안전성 및 PEDV 저해 활성의 증진을 통해 칠엽수 열매의 PEDV 치료물질로서의 활용 가능성을 제시한다.

주요어 : 칠엽수, escin, 세포독성, 가수분해, 탈아실화, oleanane-type triterpenoids, 돼지독감바이러스

학 번 : 2015-21870